Research Square

Preprints are preliminary reports that have not undergone peer review.
They should not be considered conclusive, used to inform clinical practice,
or referenced by the media as validated information.

An eclipse-calibrated periodic lunar model reproduces realistic translunar Lagrangian solutions

Massimiliano Guzzo

guzzo@math.unipd.it

Universita degli Studi di Padova

Giulio Baù

Universita degli Studi di Pisa https://orcid.org/0000-0002-9857-0866

Erica Scantamburlo

Politecnico di Torino

Giovanni B. Valsecchi

IAPS-INAF

Research Article

Keywords:

Posted Date: November 9th, 2026

DOI: https://doi.org/10.21203/rs.3.rs-11639094/v1

License: This work is licensed under a Creative Commons Attribution 4.0 International License.
Read Full License

Additional Declarations: The authors declare no competing interests.

An eclipse-calibrated periodic lunar model reproduces realistic translunar Lagrangian solutions

M. Guzzo[1], G. Baù[2], E. Scantamburlo[3], G.B. Valsecchi[4]

Abstract

Low-energy transfer orbits near the Earth-Moon Lagrangian points are key to cost-effective space missions, yet their design relies on models that oversimplify the Moon's orbital complexity, especially affecting libration orbits near L_2. Here, using a new lunar model calibrated on the Saros eclipse cycle, known since antiquity, we demonstrate the existence of Saros-periodic dynamical substitutes for L_1, L_2. These orbits reproduce the Lagrangian libration amplitudes computed from JPL ephemerides, unlike previous periodic models, while retaining periodic time dependence useful for orbital computations. The model's link to specific eclipses occurring at mirror configurations naturally identifies realistic initial conditions consistent with the real Sun-Earth-Moon system. The solar eclipse of 2 August 2027 is near such a configuration, so the model supports maneuver design for decades.

[1] *Università degli Studi di Padova, Dipartimento di Matematica "Tullio Levi-Civita", Via Trieste 63 - 35121 Padova, Italy*
[2] *Università di Pisa, Dipartimento di Matematica, Largo B. Pontecorvo 5, 56127 Pisa, Italy*
[3] *Politecnico di Torino, Department of Mechanical and Aerospace Engineering, Corso Duca degli Abruzzi 24, 10129 Torino, Italy*
[4] *IAPS-INAF, via Fosso del Cavaliere 100, 00133 Roma, Italy*

1. Introduction

Over the past decades, a diverse array of low-energy orbits derived from the circular restricted 3-body problem, as well as from periodically or quasi-periodically forced problems, has been proposed for applications in space-flight dynamics. The incorporation of these orbital trajectories into spacecraft flight plans on the one hand aims to optimize propellant efficiency, on the other hand broadens the scope of future space exploration missions [2,3,23,26]. The common aspect in the conception of low-energy orbits lies in the unique properties of the Lagrangian solutions (or points) L_1 and L_2, which are defined for any pair of celestial bodies P_0 and P_1 executing circular or elliptical motion around their barycenter. A privileged case for space flight is that of the Lagrangian solutions of the Earth-Moon system, the use of which has been proposed since the 1960s [8] and received a significant impetus since the 1980s and 1990s, thanks to the implementation of advanced dynamical systems techniques for the precise calculation of such orbits, see [1,6,12–16,22]. More recent lunar and interplanetary exploration projects have motivated the development of increasingly realistic approximations of low-energy orbits derived from the simpler models of the cislunar and translunar gravitational environment [1,18,31,35,39,43,46]. Beyond the circular and elliptic restricted 3-body problems, periodically and quasi-periodically forced problems have been considered in order to provide a transition towards a more realistic model of the cislunar and translunar gravitational environment. These include the bi-circular and quasi-bi-circular problems [1], the Hill [35] (and quasi-Hill [33]) restricted 4-body problem, and other recent formulations. Periodic models, although only relatively realistic, offer greater flexibility in applying advanced techniques from dynamical systems theory, such as continuation theorems and Floquet theory, to prove the existence of and calculate the dynamical substitutes for the Lagrangian points, as well as all the low-energy orbits associated with them [17,23,28]. Further techniques aim to grant the transition from the orbits computed using the approximate periodic model to the realistic gravitational environment [18,32,37,45].

The groundbreaking study [18] first developed quasi-periodic representations of Sun-Earth-Moon motions by analyzing the digital ephemerides of these bodies through several decades. These quasi-periodic representations were then used to compute dynamical substitutes of the Lagrangian solutions and related low-energy orbits. The frequencies appearing in these representations had been identified as linear combinations of a set of fundamental frequencies $\omega_1, \ldots, \omega_N$, which cannot be reduced to multiples of a single fundamental frequency. Denoting with $r_M(t)$ the radius vector of the Moon in a suitable geocentric reference frame, we have

$$r_M(t) = \sum_{k=(k_1,\ldots,k_N)\in\mathbb{Z}^N} r_k e^{i(k_1\omega_1+\ldots+k_N\omega_N)t}, \qquad (1)$$

with each frequency defining a period $T_j = 2\pi/\omega_j$. While quasi-periodic representations (1) of the motion of the Moon offer high-fidelity models of the real gravitational environment, they are more challenging to implement and to manage, with complexity increasing as the number N of fundamental frequencies grows. Moreover, the set of independent frequencies and related periods is not unique (any $\Omega = (\Omega_1, \ldots, \Omega_N)$ related to $\omega = (\omega_1, \ldots, \omega_N)$ by $\Omega = \Gamma\omega$, with Γ an integer matrix with $\det\Gamma = 1$, yields an alternative set of fundamental frequencies Ω). The intricate dependence of the Moon's motion on its frequencies is the reason why the search for periods associated

with lunar motion had been a fertile field of study since ancient times[47]. For instance, the search for periods in the sequences of observed eclipses led to the compilation of tables in which the eclipses themselves are arranged in series of cycles.

The study[18] employed either $N = 5$ or $N = 4$ fundamental frequencies to represent the motion of the Moon over approximately 80 decades. In the present work, we show that a quite realistic model of both the cislunar and the translunar gravitational environment can be obtained using $N = 3$ frequencies, those involved in the Saros, an eclipse cycle known since antiquity. It was discovered by the Babylonians[30], and became rather well known in the Greek world, as shown by the fact that one of the dials of the Antikythera Mechanism exploited the Saros to predict lunar eclipses[9,10]. A Saros lasts 223 synodic months, that are nearly equal to 242 nodical months and to 239 anomalistic months; the synodic month is the interval of time between two consecutive new moons, the nodical month is the interval of time between two consecutive passages at the ascending node, and the anomalistic month is the interval of time between two consecutive passages of the Moon at perigee.

Roy[40] showed that the existence of this cycle implied a near-compensation of the solar perturbations over a full Saros; then, related research showed that in the restricted, circular, spatial 3-body problem Sun-Earth-Moon there exist 8 periodic orbits of the same duration of the Saros whose dynamics closely resembles that of the real lunar orbit[49]. In these orbits the Moon passes through two Mirror Configurations (MCs); in an n-body problem, a mirror configuration is obtained if each barycentric position vector is perpendicular to every velocity vector. MCs play an essential role in the Mirror Theorem[42], whose consequence is that if a system passes through two MCs, it is in a periodic orbit.

The restricted circular, spatial Sun-Earth-Moon problem admits 16 distinct MCs, differing in ω (lunar perigee argument), f (Moon's true anomaly), and $\Delta\lambda = \lambda - \lambda'$ (difference between the geocentric true longitudes of the Moon and Sun); see Extended Data Table 1 for a unique coding of each. Of these, 8 are coplanar (with the velocities of all bodies perpendicular to the plane containing them), and 8 are collinear (with all bodies aligned and velocities perpendicular to this line). All 16 MCs are, by construction, syzygies (in the classical, extended sense; see Methods Section 7), and collinear MCs further correspond to eclipses with the Moon at perigee or apogee; see Fig. 1 for a schematic illustration of coplanar and collinear MCs, together with a non-MC syzygy and a non-syzygy eclipse. In each of the 8 periodic orbits of[49] the Moon passes through 2 MCs; since in any of these periodic orbits ω makes 3 revolutions, f makes 239 revolutions and $\Delta\lambda$ makes 223 revolutions, it is easy to determine, for a given starting MC, what MC will be reached midway through the orbit. The possibilities are: 000-222, 002-220, 020-202, 022-200, 100-322, 102-320, 120-302, 122-300; note that, e.g. 222-000 would be the same orbit as 000-222, just starting in a different phase, and that, more importantly, the time evolutions of the elements a, e, i of the orbits, e.g., 000-222 and 200-022 are the same, given that we are just exchanging the North with the South pole of the starting configurations.

The Saros-periodic orbits of[49] were computed using the Circular Restricted 3-body Problem (CR3BP) in which the mass of the Earth is equal to that of the real Earth-Moon system and the Moon is massless. Locating the Lagrangian points requires a massive Moon, which would be inconsistent with the dynamical model in which the periodic orbit 200-022 of[49] was found. To restore consistency, we turn to the classical Main Lunar Problem (MLP)[41], in which Earth, Moon and Sun have their real masses, and the barycenter of the Earth-Moon pair moves in an unperturbed ellipse about the Sun. Since a Saros lasts a non-integer number of years, implying a variation in the heliocentric radius vector of the Earth-Moon barycenter at the end of the Saros, in the model used hereafter for the lunar motion we stipulate that the Earth-Moon barycenter moves on a circle, and we call this model the Circular Main Lunar Problem (CMLP; see Methods Section 1). We find that the same MCs as in the CR3BP exist also in the CMLP. Moreover, we find that periodic orbits with the duration of the Saros also exist, with initial conditions very close to those of the periodic orbits of[49] (see Extended Data Table 2).

The motion of the real Moon is not identical to the motion in any of the above 8 periodic orbits, but it is never too different from that in at least one of them; actually, the time evolution of the elements of the real Moon appears to be currently rather close to the evolution of orbit 200-022 in the coming years: the Sun-Earth-Moon configuration at the time of the total solar eclipse of 2 August 2027 will be rather close to the 200 MC; the angular elements will be $\omega = 175^\circ.9$, $f = 2^\circ.6$, and $\Delta\lambda = 0^\circ.0$, while in the 200 MC they would be $\omega = 180^\circ$, $f = 0^\circ$, and $\Delta\lambda = 0^\circ$. The other elements will be $a = 0.002581$ au, $e = 0.07440$ and $i = 5^\circ.29$, to be compared to $a = 0.002581$ au, $e = 0.08336$ and $i = 5^\circ.69$ for the MC 200 in the periodic orbit. As shown in Extended Data Fig.1, the differences between the elements of the real lunar orbit and those of the 200-022 periodic orbit tend to remain constant on either side of the eclipse of 2 August 2027. This occurrence provides the opportunity to compute realistic dynamical substitutes of the Lagrangian solutions L_1, L_2 having the same periodicity of the Saros cycle. Then, the dynamical substitutes are computed modeling the gravitational forces in the cis-lunar and trans-lunar space using a restricted 4-body problem where the motions of the Moon and the Earth are identified by the above mentioned 200-022 periodic orbit of the CMLP. This model, not only exhibits a lunar orbit similar to the real one as explained above, but since it takes into account 3 of the 4 basic frequencies of the real lunar motion, it shares most of the small divisors, i.e. the quantities $k \cdot \omega$ of the Fourier spectrum which determine the properties of the dynamical substitute. In fact, the dynamical substitutes, as well as other related periodic or quasi-periodic orbits, may be defined as solutions of Lindstedt-Poincaré procedures (see[13–16,19,38], and the review discussion in[5]) which, as it is well known from KAM theory, depend strongly on the specific values of the small divisors. Specifically, the am-

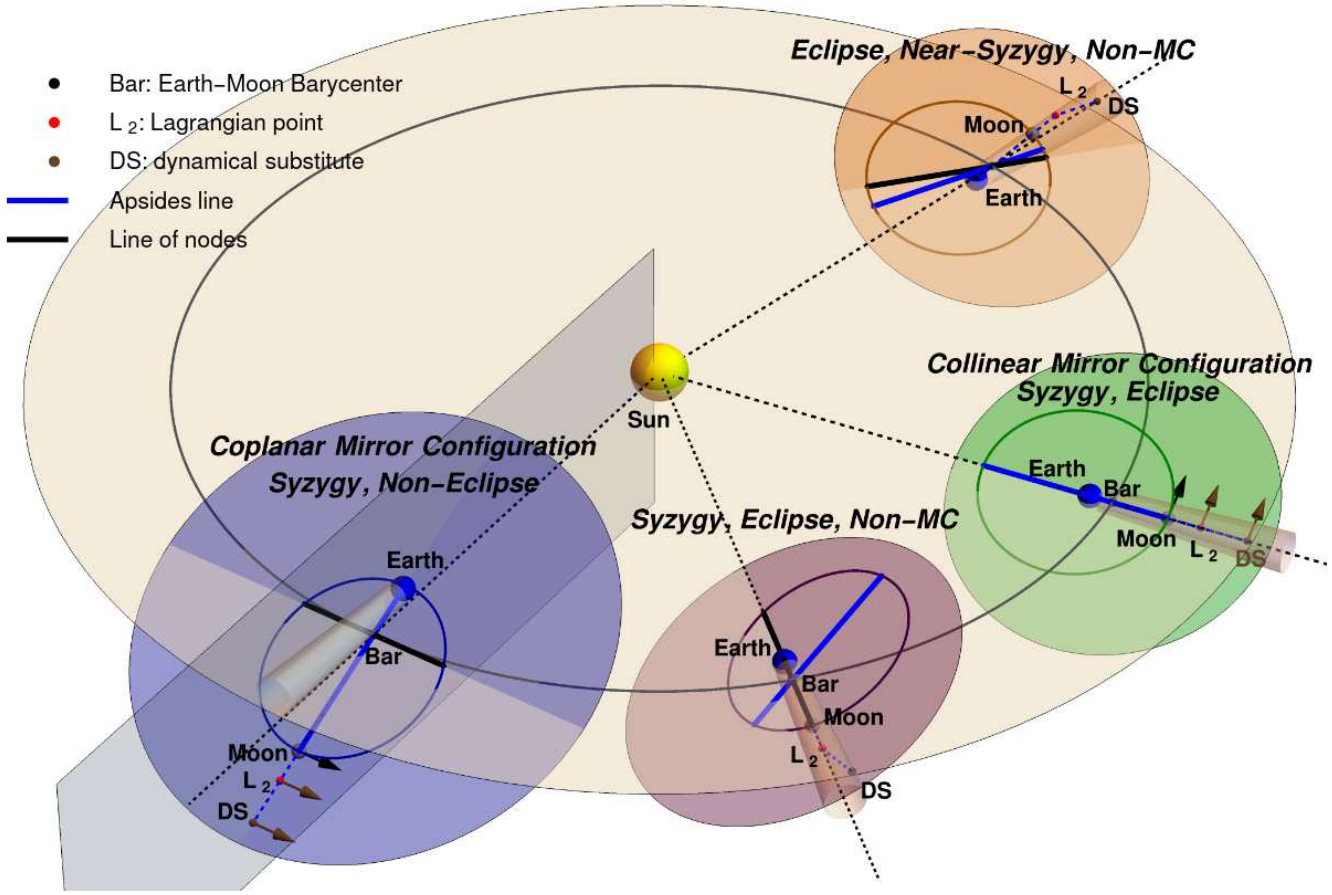


Figure 1. Mirror configurations, syzygies, and eclipses of the Sun-Earth-Moon-Lagrangian point system. Schematic representation of coplanar and collinear mirror configurations, together with two distinct eclipse-related cases, including the Lagrangian point L_2 and its dynamical substitute DS: a collinear MC, in which the Sun, Earth, Moon, L_2, and DS are all aligned, with velocities perpendicular to this alignment (green); a coplanar MC, with the Sun, Earth, Moon, L_2, and the DS in the same plane (in gray) and velocities perpendicular to the plane (blue); a syzygy in which the Sun, Earth, Moon, and L_2 are aligned but the Moon is not at perigee or apogee (purple); a generic eclipse, in which the alignment is only approximate (orange). The sizes of the bodies, their separations, and the represented angles are not to scale, and have been modified to enhance the visibility of the configurations. The classical definition of syzygies is here adopetd (see Methods Section 7).

plitudes of the Fourier representation of the solution depend mostly on the values of a subset of small divisors. Therefore, the accuracy of the dynamical substitute computed using an approximate model in representing the real system depends on how well the model reproduces the set of small divisors determining the Lindstedt-Poincaré procedure's solution. Unlike previous periodic models, the Saros-periodic dynamical substitutes of L_1, L_2 reproduce indeed the correct libration amplitudes as obtained in [1,18,27,33,37] using a quasi-periodic model, demonstrating that Saros-periodic representations of the lunar motion can effectively reproduce the dynamics of Lagrangian points within a realistic gravitational environment.

2. The four basic frequencies of the reduced lunar motion and the Saros-associated periodic orbits

We compare frequencies and amplitudes of the real lunar motion—computed via the NAFF algorithm [24] on JPL ephemerides over 3 Saros cycles—to those of the Saros periodic orbit 200-022 of the CMLP (see Methods Section 3). First, following [18], we reduce the fundamental frequencies needed to approximate the lunar ephemerides from $N = 5$ (sidereal longitudes) to $N = 4$ frequencies $\omega_1, \ldots, \omega_4$ (Extended Data Table 3), using the rotating-pulsating Cartesian reference frame centered at Earth with the Sun fixed at $(-1, 0, 0)$ (hereafter $\mathrm{SE_E}$; see Methods Section 3). This is consistent with the fact that the solar perturbations on the Moon depend on the relative phases of the three bodies, not on their longitudes. Then, we note that the real Moon's motion in the $\mathrm{SE_E}$ frame is nearly Saros-periodic: with relative corrections smaller than 4×10^{-5} and 6×10^{-6} to ω_2, ω_3, respectively, the reduced Fourier series

$$s_M(t) = \sum_{k=(k_1,k_2,k_3,0)\in\mathbb{Z}^4} r_k e^{i(k_1\omega_1+k_2\omega_2+k_3\omega_3)t}$$

is Saros-periodic. Also, $r_M(t) - s_M(t)$ is a small perturba-

tion, as can be deduced from Tables 1, 2 and Extended Data Table 4, which compare the NAFF of the Cartesian coordinates of the real lunar orbit and of the Saros-periodic orbit 200-022. Prior to examining these data, we remark that the terms present also in the periodic orbit have in many cases their peak-amplitudes of the same size order as those of the real lunar orbit. The NAFF analysis of the x and y coordinates is very similar (though not identical), while the analysis of the z coordinate presents notable differences: a smaller number of terms with peak-amplitudes larger than $5 \cdot 10^{-8}$ au (18 vs 35 for both x and y) and only 1 term in z that is in common with those for x and y: the term with period $\sim 27.321\,609$ d is absent in the periodic orbit, and it is noteworthy that for x and y its peak-amplitude is the fifth largest, while for z it is barely above the $5 \cdot 10^{-8}$ au threshold.

Analysis of the NAFF results. We start by examining the frequencies of five sidereal mean longitudes; they are (in order of decreasing absolute value): the frequency $\dot{\lambda}$ of the mean longitude of the Moon, that corresponds to the sidereal month of 27.321 662 d; the frequency $\dot{\lambda}'$ of the mean longitude of the Sun, that corresponds to the sidereal year of 365.256 363 d; the frequency $\dot{\varpi}$ of the mean longitude of the lunar perigee, that corresponds to a period of 3 232.591 8 d; the frequency $\dot{\Omega}$ of the mean longitude of the lunar node, corresponding to a period of $-6\,793.418\,3$ d; and finally the frequency $\dot{\varpi}'$ of the mean longitude of the solar perigee, corresponding to a period of 27 601 000 d (from[25]). None of these five sidereal frequencies (given also in Extended Data Table 3), appears in Tables 1, 2, and Extended Data Table 4; the reason is that the perturbations on the Moon depend on its position *relative* to the Earth and the Sun, as well as with respect to the apsidal and nodal lines, and not on the *absolute* positions of the three bodies or on the *absolute* longitudes of the apse and node. Therefore, it is more convenient to combine pairwise the five sidereal longitude frequencies to obtain ten frequencies of the longitude differences, several of which are associated with well-known periodicities. For the real lunar motion the frequencies combine so that the corresponding periods are contained in the Saros cycle an almost exact integer number of times, closely matching the integer relations found in the periodic orbit 200-022. Specifically, from the fastest frequency $\dot{\lambda}$ we can subtract:

- $\dot{\lambda}'$, obtaining $\Delta\dot{\lambda} := \dot{\lambda} - \dot{\lambda}' = 0.212\,768\,71$ rad/d, the *synodic frequency*, whose period, the synodic month, is contained in the Saros exactly 223 times both for the real lunar orbit and for the periodic orbit;
- $\dot{\varpi}$, obtaining $\dot{M} = \dot{\lambda} - \dot{\varpi} = 0.228\,027\,14$ rad/d, the *anomalistic frequency*, whose period, the anomalistic month, is contained in the Saros 238.992 times for the real lunar orbit and exactly 239 times for the periodic orbit;
- $\dot{\Omega}$, obtaining $\dot{\lambda} - \dot{\Omega} = 0.230\,895\,72$ rad/d, the *nodical frequency*, whose period, the nodical month, is contained in the Saros 241.999 times for the real lunar orbit and exactly 242 times for the periodic orbit;
- $\dot{\varpi}'$, obtaining $\dot{\lambda} - \dot{\varpi}' = 0.229\,970\,60$ rad/d, a frequency whose period of 27.321 690 d, is very close to the sidereal month of 27.321 662 d due to the very small value of $\dot{\varpi}'$; it is contained in the Saros 241.029 times for the real lunar orbit and is undefined for the periodic orbit, since in the CMLP the orbit of the Sun about the Earth-Moon barycenter is circular;

Table 1. Periods, peak-amplitudes (in au multiplied by 10^3) and the multiplicity N in the Saros, detected in the coordinate x of the real Moon and of the Saros-periodic orbit 200-022 of the CMLP represented in the S-EM reference frame (see Methods Section 3 for details).

Real Moon			Periodic orbit 200-022		
Period	Half-ampl.	N	Period	Half-ampl.	N
29.530 590	1.268 957	223.000	29.530 589	1.268 537	223.000
411.784 357	0.126 251	15.992	411.582 585	0.142 308	16.000
14.254 184	0.035 311	461.992	14.253 942	0.039 802	462.000
32.128 088	0.033 505	204.971			
27.321 680	0.012 863	241.029			
15.314 422	0.007 759	430.008	15.314 701	0.008 749	430.000
193.564 621	0.003 016	34.021			
9.843 530	0.002 533	669.000	9.843 530	0.002 699	669.000
25.231 371	0.002 314	260.997	25.231 116	0.002 666	261.000
9.394 392	0.001 449	700.984	9.394 182	0.001 842	701.000
14.833 036	0.001 181	443.963			
35.226 616	0.000 807	186.942			
15.984 617	0.000 571	411.979			
13.718 810	0.000 515	480.021			
25.826 377	0.000 504	254.984	25.824 790	0.000 636	255.000
34.475 299	0.000 261	191.016	34.478 123	0.000 331	191.000
7.252 619	0.000 248	907.992	7.252 557	0.000 293	908.000
10.116 154	0.000 244	650.971			
299.261 431	0.000 234	22.005	299.332 789	0.000 304	22.000
14.765 299	0.000 214	446.000	14.765 294	0.000 221	446.000
14.698 164	0.000 123	448.037			
14.071 043	0.000 116	468.005	14.071 199	0.000 150	468.000
35.595 753	0.000 112	185.003	35.596 332	0.000 130	185.000
126.518 668	0.000 072	52.050			
365.276 159	0.000 072	18.028			
7.005 836	0.000 070	939.976	7.005 661	0.000 100	940.000
10.337 770	0.000 066	637.016	10.338 024	0.000 083	637.000
27.555 979	0.000 063	238.980	27.553 646	0.000 072	239.000
3 232.910 076	0.000 061	2.037			
23.601 095	0.000 059	279.026			
9.642 389	0.000 058	682.955			
25.420 251	0.000 052	259.058			
7.517 423	0.000 052	876.008	7.517 490	0.000 061	876.000
13.170 918	0.000 051	499.990	13.170 643	0.000 067	500.000
9.585 210	0.000 051	687.029			

From $\dot{\lambda}'$ we can subtract:

- $\dot{\varpi}$, obtaining $\dot{\sigma} := \dot{\lambda}' - \dot{\varpi} = 0.015\,258\,433$ rad/d, a frequency first highlighted by Horrocks[21]; it is the opposite

of the frequency of the lunar perigee in the synodic frame, related to the lunar inequality known as the *evection*, and its period of 411.784 43 d is contained in the Saros 15.992 times for the real lunar orbit and exactly 16 times for the periodic orbit;

- $\dot{\Omega}$, obtaining $\dot{\lambda}' - \dot{\Omega} = 0.018\,127\,009$ rad/d, a frequency whose period of 346.620 09 d, the *eclipse year*, is contained in the Saros 18.999 times for the real lunar orbit and exactly 19 times for the periodic orbit;
- $\dot{\varpi}'$, obtaining $\dot{\lambda}' - \dot{\varpi}' = 0.017\,201\,900$ rad/d, the solar anomalistic frequency, whose period of 365.261 120 d, is very close to the sidereal year of 365.256 363 d due to the very small value of $\dot{\varpi}'$; it is contained in the Saros 18.029 times for the real lunar orbit and is undefined for the periodic orbit.

From $\dot{\varpi}$ we can subtract:

- $\dot{\Omega}$, obtaining $\dot{\varpi} - \dot{\Omega} = 0.002\,868\,575\,3$ rad/d, i.e., the frequency of the lunar argument of perigee $\dot{\omega}$, whose period of 2 190.350 5 d is contained in the Saros 3.007 times for the real lunar orbit and exactly 3 times for the periodic orbit;
- $\dot{\varpi}'$, obtaining $\Delta\dot{\varpi} := \dot{\varpi} - \dot{\varpi}' = 0.001\,943\,4568$ rad/d, a frequency whose period of 3 232.994 8 d, is very close to the ϖ period of 3 232.994 5 d due to the very small value of $\dot{\varpi}'$; it is contained in the Saros 2.037 times for the real lunar orbit and is undefined for the periodic orbit.

Finally, from $\dot{\Omega}$ we can subtract:

- $\dot{\varpi}'$, obtaining $\dot{\Omega} - \dot{\varpi}' = -0.000\,925\,118\,40$ rad/d, a frequency whose period of $-679\,1.76\,34$ d, is very close to the Ω period of $-6\,793.480\,7$ d due to the very small value of $\dot{\varpi}'$; it is contained in the Saros -0.970 times for the real lunar orbit and is undefined for the periodic orbit.

Next, we need only four fundamental frequencies, from those described above, to reproduce with their linear combinations the terms of Tables 1, 2, and Extended Data Table 4. These chosen frequencies (detailed in Extended Data Table 3) are the synodic frequency $\Delta\dot{\lambda}$; the opposite of the frequency of the lunar perigee in the synodic frame $\dot{\sigma}$; the frequency of the lunar argument of perigee $\dot{\omega}$; the difference of the frequencies of the lunar and solar perigees $\Delta\dot{\varpi}$. Note that the fourth frequency is present only in the real lunar orbit, and not in the periodic orbit, for which ϖ' is undefined.

The fundamental frequencies are identified through the following procedure. Extended Data Table 5, Extented Data Table 7 and Table 6 contain some of the same data contained in the corresponding Tables 1, 2 and Extended Data Table 4. In particular, columns 1 and 2 contain the same data as columns 1 and 3 of Tables 1, 2 and Extended Data Table 4, while column 3 specifies whether the frequency is detected in both the real lunar orbit and in the periodic orbit, or only in the former. The data in columns 4 and 5 are obtained as follows:

Table 2. Periods, peak-amplitudes and the multiplicity N in the Saros as in Table 1, detected in the coordinate z.

Real Moon			Periodic orbit 200-022		
Period	Half-ampl.	N	Period	Half-ampl.	N
27.212 221	0.115 065	241.999	27.212 072	0.123 412	242.000
2 190.319 549	0.009 351	3.007	2 195.102 903	0.011 318	3.000
32.280 778	0.004 265	204.001	32.280 987	0.004 581	204.000
13.691 158	0.003 168	480.991	13.690 897	0.003 830	481.000
188.201 314	0.001 511	34.991	188.152 039	0.001 826	35.000
29.402 755	0.000 998	223.970			
25.325 450	0.000 928	260.028			
14.666 428	0.000 697	449.006	14.666 640	0.000 842	449.000
35.410 248	0.000 247	185.972			
9.571 707	0.000 227	687.999	9.571 688	0.000 260	688.000
313.059 023	0.000 131	21.035			
9.146 496	0.000 130	719.983	9.146 280	0.000 177	720.000
27.905 587	0.000 114	235.986	27.903 904	0.000 156	236.000
14.865 504	0.000 103	442.993	14.865 285	0.000 124	443.000
124.204 480	0.000 079	53.020			
24.035 515	0.000 061	273.983	24.034 019	0.000 083	274.000
27.321 609	0.000 052	241.030			

- for frequencies contained both in the real lunar orbit and in the periodic orbit (denoted by 'Yes' in column 3), we take the integer that is nearest to the value reported in column 2, and find the linear combination, with integer coefficients, of the values 223, 16 and 3 (the number of times that $2\pi/\Delta\dot{\lambda}$, $2\pi/\dot{\sigma}$ and $2\pi/\dot{\omega}$ are contained in a Saros for the periodic orbit) that is equal to that integer; the coefficients thus found are reported in column 4 and are then used to find the combination of longitude rates given in column 5;
- for frequencies contained only in the real lunar orbit (denoted by 'No' in column 3), the procedure is essentially the same, the only difference being that now the linear combination matching the value of column 2 must include also the non-integer 2.037, corresponding to $\Delta\dot{\varpi}$.

A few examples will clarify the procedure; to this purpose, we discuss the first five frequencies present in Extended Data Table 5, that actually are the same as the first five of Extended Data Table 6. The first two frequencies are simply $\Delta\dot{\lambda}$ and $\dot{\sigma}$, so the longitude rate combinations are immediately found from Extended Data Table 3. The third frequency is contained in the Saros 461.992 times; the nearest integer is 462, that is readily obtained from 223 and 16 as $462 = 2 \cdot 223 + 16$ (see column 4); then, the frequency is obtained as follows:

$$2\Delta\dot{\lambda} + \dot{\sigma} = 2\dot{\lambda} - 2\dot{\lambda}' + \dot{\lambda}' - \dot{\varpi} = 2\dot{\lambda} - \dot{\lambda}' - \dot{\varpi},$$

as shown in column 5. The fourth and fifth frequencies are absent from the periodic orbit. In particular, the fourth is contained in the Saros 204.971 times; the nearest integer is 205, which is obtained from 223, 16 and 2 (rounded from 2.037) as $205 = 223 - 16 - 2$ (see column 4); then, the frequency is

obtained as follows:

$$\Delta\dot{\lambda}-\dot{\sigma}-\Delta\dot{\varpi}=\dot{\lambda}-\dot{\lambda}'-\dot{\lambda}'+\dot{\varpi}-\dot{\varpi}+\dot{\varpi}'=\dot{\lambda}-2\dot{\lambda}'+\dot{\varpi}',$$

as shown in column 5. The fifth frequency is contained in the Saros 241.029 times; the nearest integer is 241, which is obtained from 223, 16 and 2 as $241=223+16+2$; then, the frequency is obtained as follows:

$$\Delta\dot{\lambda}+\dot{\sigma}+\Delta\dot{\varpi}=\dot{\lambda}-\dot{\lambda}'+\dot{\lambda}'-\dot{\varpi}+\dot{\varpi}-\dot{\varpi}'=\dot{\lambda}-\dot{\varpi}',$$

that, as discussed before, is very close to the sidereal frequency of the Moon.

3. Saros-periodic dynamical substitutes in a restricted 4-body problem

We provide a Saros-periodic dynamical substitute in a restricted 4-body problem where the spacecraft is attracted gravitationally by the Sun, the Earth and the Moon, whose motions are assigned by a solution of the CMLP: the Sun and the Earth-Moon barycenter perform a circular motion around their common barycenter, while the position vector $\Delta(t)$ from the Earth to the Moon is the solution 200-022 of the CMLP. Using the Sun-(Earth-Moon barycenter) synodic reference frame, which rotates with frequency n' with respect to the sidereal one (see Methods Section 1), the solution $\Delta(t)$ is Saros-periodic, and the position vector δ from the Moon to the spacecraft satisfies:

$$\begin{aligned}\ddot{\delta}=F(\delta,\dot{\delta},\Delta(t)):=&-2n'e_3\wedge\dot{\delta}+n'^2(\delta_x,\delta_y,0)\\&-\mathscr{G}m_S\left[\frac{\delta+\frac{m_E}{m_M+m_E}\Delta-\rho}{\left\|\delta+\frac{m_E}{m_M+m_E}\Delta-\rho\right\|^3}-\frac{\frac{m_E}{m_M+m_E}\Delta-\rho}{\left\|\frac{m_E}{m_M+m_E}\Delta-\rho\right\|^3}\right]\\&-\mathscr{G}m_E\left[\frac{\delta+\Delta}{\|\delta+\Delta\|^3}-\frac{\Delta}{\|\Delta\|^3}\right]-\mathscr{G}m_M\frac{\delta}{\|\delta\|^3}\end{aligned}\tag{2}$$

where m_S,m_E,m_M are the masses of the Sun, the Earth and the Moon; $\mathscr{G}$ is the gravitational constant; $e_3=(0,0,1)$; $\rho=(-1,0,0)$ is the position vector from the Sun to the Earth-Moon barycenter, and:

$$\Delta(t)=\sum_{n=0}^{N}a_ne^{i\nu_nt};\tag{3}$$

the amplitudes a_n and frequencies ν_n are computed from the NAFF of the Saros-periodic solution 200-022 of the CMLP, see Methods Section 3.

The Saros-periodic dynamical substitute (DS hereafter) is provided by a Fourier polynomial of N_S terms:

$$\mathscr{E}=\sum_{n=0}^{N_S}\varepsilon_ne^{i\nu_nt},\tag{4}$$

which yields the position vector $\delta(t)$ as a deviation from a formal Lagrangian solution δ_{L_i}: $\mathscr{E}(t)=\delta(t)-\delta_{L_i}(t)$. For L_1,L_2 the formal Lagrangian solution is collinear with the Earth and the Moon:

$$\delta_{L_i}(t)=\alpha_{L_i}\Delta(t),\tag{5}$$

and the parameter α_{L_i} is computed as in the Earth-Moon CR3BP as a solution of:

$$m_E(1+\alpha)+m_M\alpha-m_E\frac{(1+\alpha)}{|1+\alpha|^3}-m_M\frac{\alpha}{|\alpha|^3}=0.\tag{6}$$

By linearizing Eq. (2) at $\delta_{L_i}(t)$ we obtain

$$\ddot{\mathscr{E}}=\sum_{k=0}^{N_S}C_ke^{i\nu_kt}+\Big(\sum_{k=0}^{N_S}D_ke^{i\nu_kt}\Big)\mathscr{E}-2n'e_3\wedge\dot{\mathscr{E}}\tag{7}$$

where the vectors C_k and the matrices D_k have entries provided by a frequency analysis of the known term and of the variational matrix of the linearization at $r_{L_i}(t)$ of the right–hand side of Eq. (2). The CMLP and the restricted four-body problem here defined have the remarkable property that when the parameter α_{L_i} is chosen as a solution of Eq. (6), the amplitudes C_k of the known term in Eq. (7) are considerably reduced compared to other possible choices, see Methods Section 2. Finally, Eq. (7) is solved by fixing N_S and the corresponding solution (4) provides an approximation for the DS. Since all the frequencies ν_n in Eq. (3) are integer multiples of $\Omega_{\mathscr{S}}=(\Delta\dot{\lambda}/223)$, the DS $\mathscr{E}(t)$ is Saros periodic as well. Moreover, the initial conditions of the DS, the Sun, the Earth and the Moon provide a MC[42].

In the top panels of Fig. 2 we represent the projections of our best computation of $\mathscr{E}(t)$ for the Lagrangian point L_2, obtained for $N_S=558$, on the x-y (top-left) and x-z (top-right) planes of a reference frame which is centered at the formal Lagrangian solution, and is rotating-pulsating to maintain the Earth and the Moon on the x axis, with mutual distance equal to 1. The projection of the periodic orbit along a complete Saros cycle (orange, top-left panel) overlaps remarkably with the representation of the dynamical system obtained for the complete non-periodic dynamical model (see Figure 14 of[33]) showing the excellent reproduction of the libration amplitudes in the x, y and z directions. In particular, for L_2, the Saros-periodic orbit replicates the complete libration amplitude in the y variable, whereas the best previously available periodic model (the quasi-bicircular problem) reproduced merely 1/3 of the libration, as reported in[33]. The largest value of $y>0$ is reached in 4 synodic months. In the bottom panel of the figure we also represent the residuals of the computation of $\mathscr{E}(t)$, given by

$$\mathscr{R}(t):=\ddot{\mathscr{E}}-[F(\mathscr{E}(t)+\delta_{L_i}(t),\dot{\mathscr{E}}(t)+\dot{\delta}_{L_i}(t),\Delta(t))-\ddot{\delta}_{L_i}(t)],\tag{8}$$

where F is the acceleration field defined in (2). The residuals, computed using different orders of approximations N_S, are represented in Extended Data Fig.3: from $N_S=100$ to $N_S=558$ we appreciate a reduction of the residuals of about a factor 100,

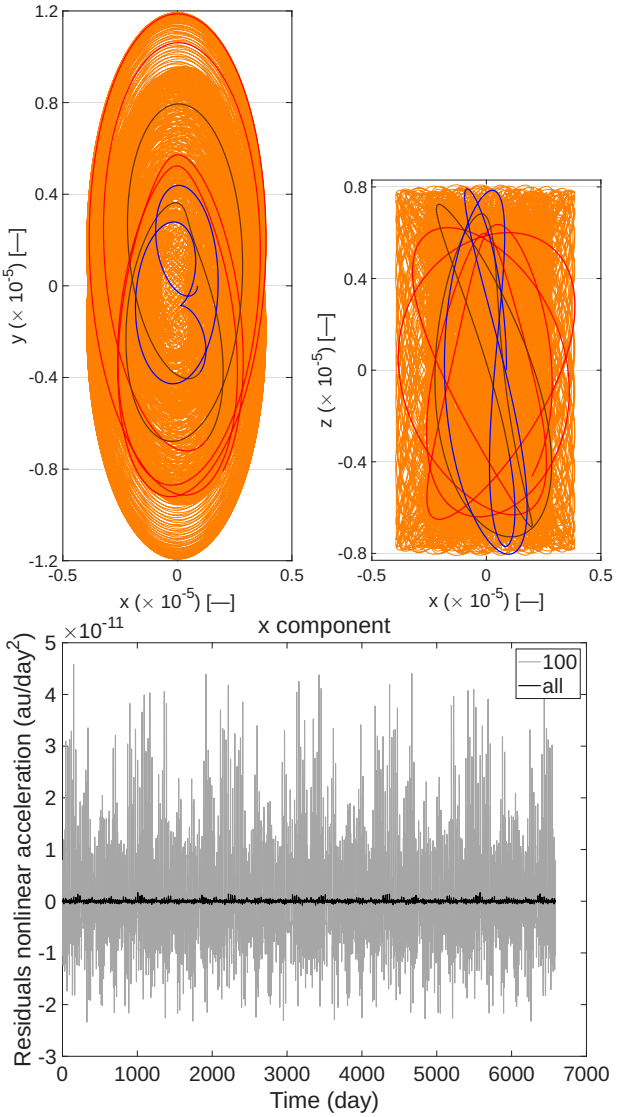


Figure 2. Top panels: projections of the DS L_2 on the x-y (top-left) and x-z (top-right) planes of a reference frame centered at the formal Lagrangian solution and rotating-pulsating to maintain the Earth and the Moon on the x axis, with mutual distance equal to 1. The projected curves are represented in orange along a full Saros cycle, in blue, brown along the first and second synodic months, and in red along the third and fourth synodic months. Bottom panel: time evolution of the residuals $\mathscr{R}_x(t)$ on the acceleration of the numerically computed DS L_2 defined in Eq. (8), for $N_S = 100$ and the maximum number of considered frequencies $N_S = 558$.

corresponding to residuals smaller than 2.26 10^{-13} au/day^2. Analogous results, with remarkable reproduction of the libration amplitudes in the Saros periodic model, are obtained for the Lagrangian point L_1 (see Extended Data Fig.2, Fig.3).

4. Discussion

Periodic models of the Sun-Earth-Moon motion offer substantial computational advantages in the analytical computation of low-energy orbits, and recent research has sought models increasingly faithful to the real motion of the system. A standard benchmark for this fidelity is the agreement between the librations of the dynamical substitute of the lunar Lagrangian point L_2 computed with JPL ephemerides and with a periodic model. Historically important models, such as the CR3BP and Hill's problem, as well as some more recent ones, do not reproduce the vertical component (z coordinate of 2) of the libration at all and capture less than half of the horizontal components (x, y coordinates of 2). The difficulty is intrinsic to the real system: the forcing terms acting on the dynamical substitute of the real L_2 require a large set of frequencies in the Fourier representation of the real lunar motion, which a periodic model must capture with a much smaller set. For the next decades, however, the most important of these terms are reproduced by linear combinations of only three basic frequencies: $\Delta\dot{\lambda} = \dot{\lambda} - \dot{\lambda}'$, $\dot{\sigma} = \dot{\lambda}' - \dot{\varpi}$ and $\dot{\omega} = \dot{\varpi} - \dot{\Omega}$. These match those of Saros-periodic motions in the CMLP, confirming that it represents the real lunar motion with high fidelity over several decades. Accordingly, the dynamical substitutes of both L_1 and L_2, computed in a restricted 4-body problem with a Saros-periodic lunar motion, are themselves Saros-periodic and closely reproduce the libration amplitudes obtained with the real ephemerides. Given the mathematical simplicity of periodic models and the natural identification of initial conditions provided by the link with the mirror configurations of the real Sun-Earth-Moon system, we propose the Saros-periodic model as the basis for future orbit design around the cislunar and translunar points L_1 and L_2. In particular, Saros-periodic dynamical substitutes can serve as the starting point for a comprehensive family of low-energy transfers to and from L_1 and L_2. Since the current epoch is close to the total solar eclipse of 2 August 2027, the model remains valid for at least the next few decades, justifying the development of efficient maneuver design and testing protocols that minimize residuals with respect to a realistic ephemerides model.

Methods

1. The Circular Main Lunar Problem and the Saros-periodic orbit 200-022

The 200-022 Saros-periodic solution for the motion of the Moon, previously computed in a circular restricted three-body problem[49], is here recomputed in a restricted version of the Main Lunar Problem where the barycenter of the Earth-Moon system is constrained on a circular heliocentric orbit, which we call the Circular Main Lunar Problem. The CMLP is defined as follows. Consider the general three-body problem defined by the Sun, the Earth and the Moon with masses m_S, m_E, m_M respectively. Then, we write the equations of motion in an inertial reference frame centered at the barycenter of the system using the Jacobi coordinates, i.e. the vectors $\Delta = r_M - r_E$ and $\rho = r_S - r_B$, where $r_B = (m_E r_E + m_M r_M)/(m_E + m_M)$ is the barycenter of the Earth-Moon system (see, e.g.[36], Eq.s (7.2) and (7.3), Chapter 2). A restricted Main Lunar problem is first obtained by replacing the equation of motion for ρ with:

$$\ddot{\rho} = -\frac{\mathscr{G}(m_S + m_E + m_M)}{\|\rho\|^3}\rho \tag{9}$$

and then the CMLP is obtained by selecting for Eq. (9) the circular solution

$$\rho(t) = -(\cos n't, \sin n't, 0)\ ,\ n' = \sqrt{\mathscr{G}(m_S + m_M + m_E)}. \tag{10}$$

Finally, the equation of motion for Δ is:

$$\begin{aligned}\ddot{\Delta} = &-\frac{\mathscr{G}(m_E + m_M)}{\|\Delta\|^3}\Delta \\ &+\mathscr{G}m_S\left[\frac{\rho - \frac{m_E}{m_E+m_M}\Delta}{\left\|\rho - \frac{m_E}{m_E+m_M}\Delta\right\|^3} - \frac{\rho + \frac{m_M}{m_E+m_M}\Delta}{\left\|\rho + \frac{m_M}{m_E+m_M}\Delta\right\|^3}\right].\end{aligned} \tag{11}$$

The orbit 200-022, previously computed in a circular restricted three-body problem[49], is here recomputed using the same methods applied to the equations of motion (11). By representing $\Delta(t)$ for this solution in a synodic reference frame which is uniformly rotating around the vertical axis with angular velocity n', we obtain the Saros periodic function that is inserted into Eq. (2) for the computation of the dynamical substitutes.

2. Definition of the formal Lagrangian solutions $\delta_{L_i}(t)$

We expand at $\mathscr{E} = 0$ the right-hand side of the differential equation:

$$\ddot{\mathscr{E}} = F(\mathscr{E} + \alpha\Delta, \dot{\mathscr{E}} + \alpha\dot{\Delta}, \Delta(t)) - \alpha\ddot{\Delta} \tag{12}$$

where F is defined in Eq. (2) and $\ddot{\Delta}$ is replaced by the right-hand side of Eq. (11) incremented by the Coriolis and centrifugal forces $-2n'e_3 \wedge \dot{\Delta} + n'^2(\Delta_x, \Delta_y, 0)$. We then define α in order to cancel from the known-term $F(\alpha\Delta, \alpha\dot{\Delta}, \Delta(t)) - \alpha\ddot{\Delta}$ the contributions which are singular in the vector $\Delta := r_M - r_E$:

$$\mathscr{G}\left(-m_E\frac{(1+\alpha)}{|1+\alpha|^3} + m_E - m_M\frac{\alpha}{|\alpha|^3} + \alpha(m_E + m_M)\right)\frac{\Delta}{\|\Delta\|^3}, \tag{13}$$

which is achieved by choosing α as a solution of Eq. (6).

3. NAFF of the lunar motion

The Fourier representation of the lunar ephemerides is obtained from the numerical analysis of fundamental frequencies (NAFF) algorithm[24] provided by the software TRIP[11]. We analyze with TRIP the lunar ephemerides corresponding to an interval of time defined by three consecutive Saros cycles belonging to the Saros Series 136 (the epochs of the eclipses in the Saros Series 136 are given in[44]). The considered time interval ranges from the total solar eclipe of 07-22-2009 to the total solar ecplipse of 08-24-2063. The central Saros begins with the total solar eclipse of 08-02-2027, so that our analysis can be of interest for the next space missions. The Moon's and Earth's ephemerides are downloaded from the NASA digital catalog[29] using a stepsize of 12 hours.

To compare the frequencies and related amplitudes of the real lunar motion with those of the periodic orbit 200-022, we adopt as in[18] a rotating-pulsating reference frame (denoted by S-EM) centered at the Earth, whose axes are rotated as in the synodic reference frame of the Sun-(Earth-Moon barycenter), and the mutual distances are rescaled by the distance of the Earth-Moon barycenter from the Sun. In particular, in the S-EM, the length unit is the distance of the Sun from the Earth-Moon barycenter, while the time unit is the day.

The NAFF is then applied to both Moon's relative position Δ given by the Saros-periodic solution 200-022 of the CMLP and the corresponding quantity $\Delta^{\text{S-EM}}$ of the real orbit of the Moon represented in the S-EM reference frame. Extended Data Fig.4 shows the spectra of the three components of $\Delta^{\text{S-EM}}$, which are characterized by a multiplet structure, where the height of each multiplet determines the asymptotic decay of the spectrum at large frequencies, and inside each multiplet we find many peaks of very close frequencies packed together. As will be explained in Methods Section 5, this structure guides the choice of the frequencies selected for the solution of Eq. (7).

4. NAFF of the linearized Eq. (7)

Let

$$C := \sum_{k=0}^{N_S} C_k e^{i\nu_k t}, \quad D := \sum_{k=0}^{N_S} D_k e^{i\nu_k t}.$$

Then, from Eq. (7), we have

$$C = F(\alpha_{L_i}\Delta, \alpha_{L_i}\dot{\Delta}, \Delta) - \alpha_{L_i}\ddot{\Delta}, \tag{14}$$

$$D = \frac{\partial F}{\partial \delta}(\alpha_{L_i}\Delta, \alpha_{L_i}\dot{\Delta}, \Delta), \tag{15}$$

where $\Delta := \Delta(t)$ is represented by a Fourier series provided by the NAFF of the orbit 200-022. The NAFF is then applied to the right–hand sides of Eqs. (14), (15), to obtain the frequencies and related amplitudes for the components of the vector C and for the entries of the symmetric matrix D. The spectra for L_1 and L_2 are shown in Extended Data Fig.5 and Fig.6.

5. The Galerkin method for the solution of the linearized Eq. (7)

We look for solutions of the linearized Eq. (7) in the form of a Lindstedt series (see [13–16,19,38], and the review discussion in [5]), which, in the periodic case, is a Fourier series

$$\mathscr{E}(t) = \sum_{k\geq 0} \varepsilon_k e^{i\nu_k t}, \tag{16}$$

where the frequencies ν_k are all the integer multiples of the Saros frequency $\Omega_{\mathscr{S}}$. We solve Eq. (7) by implementing a Galerkin method, which provides as an approximate solution a Fourier polynomial whose harmonics are the solutions of a linear non-homogeneous system of equations of finite dimension. The implementation of the Galerkin method works as follows.

- First, using (16), Eq. (7) is transformed into

$$\begin{aligned} &-\sum_{k\geq 0} \nu_k^2 \varepsilon_k e^{i\nu_k t} - \Big(\sum_{k'\geq 0} D_{k'} e^{i\nu_{k'} t}\Big)\Big(\sum_{k''\geq 0} \varepsilon_{k''} e^{i\nu_{k''} t}\Big) + \\ &+\sum_{k\geq 0} 2i\nu_k \Omega (e_3 \times \varepsilon_k) e^{i\nu_k t} = \sum_{k=0} C_k e^{i\nu_k t}, \end{aligned} \tag{17}$$

  whose unknowns are the vectors $\varepsilon_k \in \mathbb{R}^3$. Since all the frequencies ν_k are integer multiples of $\Omega_{\mathscr{S}}$, the multiplication of Fourier series in the left–hand side of Eq. (17) is again expanded as a Fourier series whose frequencies are integer multiples of $\Omega_{\mathscr{S}}$.

- Then, we equate the Fourier coefficients on both sides of Eq. (17) for each ν_k to obtain

$$-\nu_k^2 \varepsilon_k - \sum_{\substack{k',k''\geq 0 \\ \nu_{k'}+\nu_{k''}=\nu_k}} D_{k'} \varepsilon_{k''} + 2i\nu_k \Omega (e_3 \times \varepsilon_k) = C_k, \tag{18}$$

  which collectively constitutes a countable system of linear non-homogeneous algebraic equations. Though the system is linear, its solution is not straightforward due to the infinite number of equations and unknowns $\varepsilon_0, \varepsilon_1, \ldots$. Moreover, the terms $\varepsilon_0, \varepsilon_1, \ldots$ of an algebraic solution must sum to a function which is analytic in time, i.e.

$$\sum_{k\geq 0} |\varepsilon_k| e^{-\sigma|\nu_k|} < +\infty \tag{19}$$

  for some $\sigma > 0$. The convergence condition (19) justifies the calculation of approximate solutions:

$$\mathscr{E}(t) = \sum_{k=0}^{N_S} \varepsilon_k e^{i\nu_k t} \tag{20}$$

  when the norm of remainder term $\sum_{k=N_S+1}^{+\infty} \varepsilon_k e^{i\nu_k t}$ is majorated by a function which converges exponentially to zero as the order of approximation N_S increases.

- Following the Galerkin method, we compute approximate solutions in the form (20) by projecting both sides of Eq. 17 on a finite set $\mathscr{L}$ of frequencies. The accuracy of the approximate solution depends on the choice of the frequency set $\mathscr{L}$, which is particularly critical in this case (see below).

- Finally, we verify that the remainder term is negligible. This is done by computing the residuals of the computed function (20) as a solution of Eq. (7). Actually, we compute also the residuals, defined in Eq. (8), as a solution of the non-linear equation of motion.

The implementation of this version of the Galerkin method for the computation of the dynamical substitutes of L_1, L_2 encounters specific difficulties due to the peculiar Fourier spectra of the functions defined in the right-hand sides of (14) and (15), see Extended Data Fig.5 and Fig.6, whose decay with respect to $|\nu_k|$ is very slow, and therefore a large number N_S is required to obtain a reliable representation of the solution by a Fourier polynomial. Moreover, as it is typical for functions which are computed on the ephemerides of celestial bodies [20], their Fourier spectra are organized in multiplets, where the height of each multiplet determines the asymptotic decay of the spectrum at large frequencies, and inside each multiplet we find many peaks of very close frequencies packed together. Since the ratio between the largest frequencies represented in the panels of Extended Data Fig.6 and the Saros frequency $\Omega_{\mathscr{S}}$ is of $N \sim 1000$, it is not convenient to solve the system of Eqs. (18) by ordering the frequency as $\nu_k = k\Omega_{\mathscr{S}}$. Indeed, proceeding in this manner would be definitely not convenient, as, due to the multiplet structure of the spectra, most of the frequencies defined in this way would not have an amplitude larger than 10^{-16} au/d. Also, our aim is to obtain a reasonable balance between the accuracy of the solution and the number of frequencies required to represent it. Therefore, we first order the frequencies detected by the NAFF of C_j and $D_{i,j}$ according to the amplitudes of the correspondent harmonics (see Methods Section 6 for more details). Then, by arguing that also the Fourier spectrum of the dynamical substitute has a multiplet structure whose dominant terms correspond to the frequencies already detected in the NAFF of the spectra of the components of C and entries of D, we solve Eq. (18) with $\mathscr{L}$ containing all these frequencies, as well as a selection of their linear combinations which provide the largest coefficients in the product of the terms $D_{k'}$ and $\varepsilon_{k''}$ in Eq. (17), and did not appear in the previous list. In this way, for L_2 we obtain a reliable solution using a Fourier polynomial with $N_S \sim 500$.

6. Numerical implementation of the solution of the linearized Eq. (7)

The linear system of Eqs. (18) is represented using as input parameters for m_s, m_E, m_M the masses of the Sun, Earth and Moon taken from JPL ephemerides. Also, the period of the Saros is $T_{\mathscr{S}} = 6\,585.321\,347$ d, with associated frequency $\Omega_{\mathscr{S}} = 2\pi/T_{\mathscr{S}}$.

NAFF is applied to the components of the vector C and to the entries of the matrix D (this matrix is symmetric, so only the entries $D^{(11)}$, $D^{(12)}$, $D^{(13)}$, $D^{(22)}$, $D^{(23)}$, $D^{(33)}$ are considered). For each fundamental frequency f_k, $k = 1, \ldots, N$, where N depends on the analyzed quantity, the norm of the corresponding amplitude is provided, along with the real and imaginary parts of the amplitude. These data are reported in the same row of

the output file, which consists of 5 columns (the first one contains an increasing integer index starting from 1). The number of rows of the output file (excluding the first two which are not relevant), is equal to $2N$, because for each frequency $f_k > 0$, an additional row for $-f_k$ is given, where the norm and the real part of the amplitude have the same values as for f_k, while the imaginary part has opposite sign.
Let N_t be the number of all positive frequencies obtained by the NAFF for $C^{(1)}$, $C^{(2)}$, $C^{(3)}$, $D^{(i,j)}$, $1 \le i \le j \le 3$, and the Cartesian components of $r_M(t) - r_E$. The rows in the output files of the NAFF corresponding to these frequencies are sorted by decreasing values of the norms of the corresponding amplitudes. Then, the nearest integer n_ℓ to the ratio $f_\ell/\Omega_{\mathscr{S}}$, $\ell = 1,\dots,N_t$, is computed. If more than one row refers to the same multiple of the Saros frequency $\Omega_{\mathscr{S}}$, only the row with the highest norm of the amplitude is kept in the list. In this way, we get a list of frequencies $n_m\Omega_{\mathscr{S}}$, $m = 1,\dots,\tilde{N}_t \le N_t$, sorted by the decreasing values of the norm of the related amplitudes. Finally, for each of the nine quantities $C^{(1)}$, $C^{(2)}$, $C^{(3)}$, $D^{(i,j)}$, $1 \le i \le j \le 3$, we build an array, where the first column is made by the integers n_m, $\ell = 1,\dots,\tilde{N}_t$, and the other three columns are computed as follows. If n_m is equal to the nearest integer to $f_k/\Omega_{\mathscr{S}}$, where f_k is one of the fundamental frequencies of the considered quantity, then in the 2nd, 3rd and 4th columns of the m-th row we report the norm, real and imaginary parts of the amplitude related to that frequency, otherwise we write 0.

7. Syzygies, coplanar and collinear mirror configurations, eclipses

We here provide the classical definition of syzygies of the Sun-Earth-Moon system (which is different from some modern definitions given for generic 3-body problems, identifying syzygies as alignment of all the bodies), as well as of coplanar and collinear Mirror configurations and of eclipses.

Let the ecliptic be the plane of the Keplerian orbit of the Earth-Moon barycenter Γ about the Sun, let Ω, ω, f be the angular elements of the orbit of the Moon computed with respect to Γ, and Ω', ω', f' those of the Sun. Γ-centered latitude and longitude of the Moon are given by

$$b = \arcsin[\sin(\omega + f)\sin i],$$

$$l = \Omega + 2\arctan\left(\frac{\sin(\omega+f)\cos i}{\cos(\omega+f)+\cos b}\right),$$

and those of the Sun are

$$b' = \arcsin[\sin(\omega' + f)'\sin i'],$$

$$l' = \Omega' + 2\arctan\left(\frac{\sin(\omega'+f')\cos i'}{\cos(\omega'+f')+\cos b'}\right).$$

Then, we have

- a syzygy when

$$\sin(l - l') = 0;$$

- a collinear MC when

$$\sin(l - l') = 0, \qquad \sin M = 0, \qquad \sin\omega = 0;$$

- a coplanar MC when

$$\sin(l - l') = 0, \qquad \sin M = 0, \qquad \cos\omega = 0;$$

- an eclipse when

$$\sin(l - l') \lesssim 0.01, \qquad \sin(l' - \Omega) \lesssim 0.3.$$

Finally, we recall that the latitude b, computed from the orbital elements:

$$b = \arcsin[\sin(\omega + f)\sin i],$$

has no quadrant problem. The true longitude λ,

$$\lambda = \Omega + \omega + f,$$

differs from the longitude l computed from the coordinates:

$$\cos l = \frac{x}{r\cos b}, \qquad \sin l = \frac{y}{r\cos b}.$$

To pass from orbital elements to l, one can use the relations

$$\begin{aligned}\cos l &= \tfrac{\cos\Omega\cos(\omega+f) - \sin\Omega\sin(\omega+f)\cos i}{\cos b},\\ \sin l &= \tfrac{\sin\Omega\cos(\omega+f) + \cos\Omega\sin(\omega+f)\cos i}{\cos b},\end{aligned}$$

which give the correct quadrant. A more compact relation, also unaffected by quadrant ambiguity, is

$$l = \Omega + 2\arctan\left(\frac{\sin(\omega+f)\cos i}{\cos(\omega+f)+\cos b}\right).$$

Acknowledgments

E. Scantamburlo wishes to acknowledge Università di Pisa and Politecnico di Torino, as her contribution to this paper was carried out in full during her tenure at that institutions.

References

[1] Andreu, M.A. The quasi-bicircular problem. Ph.D. dissertation, Universitat de Barcelona, Spain (1998).

[2] Angelopoulos, V. The ARTEMIS Mission. *Space Science Reviews*. **165**, 3-25 (2011).

[3] Baker-McEvilly, B., Bhadauria, S., Canales, D., Frueh, C. A comprehensive review on Cislunar expansion and space domain awareness. *Progress in Aerospace Sciences*. **147**, 101019 (2024).

[4] Belbruno, E.A., Miller, J.K. Sun-Perturbed Earth-to-Moon Transfers with Ballistic Capture. *Journal of Guidance, Control, and Dynamics*. **16**, 4, 770-775 (1993).

[5] Belló, M., Gómez, G., Masdemont, J.J. Invariant Manifolds, Lagrangian Trajectories and Space Mission Design. In: Perozzi, E., Ferraz-Mello, S. (eds) Space Manifold Dynamics. Springer, 1-96 (2010).

[6] Breakwell, J.V., Brown, J.V. The 'Halo' family of 3-dimensional periodic orbits in the Earth-Moon restricted 3-body problem. *Celestial Mechanics*. **20**, 389-404 (1979).

[7] Conley, C.C. Low energy transit orbits in the restricted three-body problem. *SIAM J. of Appl. Math.*. **16**, 4, 732-746 (1968).

[8] Farquhar, R.W. Station-Keeping in the Vicinity of Collinear Libration Points with an Application to a Lunar Communications Problem. In: Space Flight Mechanics, Vol. 11 of Science and Technology Series, American Astronautical Society, New York, 519-535 (1966).

[9] Freeth, T. et al. Decoding the ancient Greek astronomical calculator known as the Antikythera Mechanism. *Nature*. **444**, 587–591 (2006).

[10] Freeth, T., Jones, A., Steele, J.M., Bitsakis, Y. Calendars with Olympiad display and eclipse prediction on the Antikythera Mechanism. *Nature*. **454**, 614–617 (2008).

[11] Gastineau, M., Laskar, J. TRIP: a computer algebra system dedicated to celestial mechanics and perturbation series. *ACM Communications in Computer Algebra*. **44**, 3/4 (2011).

[12] Gómez, G., Jorba, À., Masdemont, J.J., Simó, C. Study of the transfer between halo orbits. *Acta Astronautica*. **43**, 9-10, 493-520 (1998)

[13] Gómez, G., Llibre, J., Martínez, R., Simó, C. *Dynamics and Mission Design Near Libration Points. Vol. I Fundamentals: The Case of Collinear Libration Points*. World Scientific Publishing Company (2001).

[14] Gómez, G., Llibre, J., Martínez, R., Simó, C. *Dynamics and Mission Design Near Libration Points. Vol. II Fundamentals: The Case of Triangular Libration Points*. World Scientific Publishing Company (2001).

[15] Gómez, G., Jorba, À., Masdemont, J.J., Simó, C. *Dynamics and Mission Design Near Libration Points. Vol. III Advanced Methods for Collinear Points*. World Scientific Publishing Company (2001).

[16] Gómez, G., Jorba, À., Masdemont, J.J., Simó, C. *Dynamics and Mission Design Near Libration Points. Vol. IV Advanced Methods for Triangular Points*. World Scientific Publishing Company (2001).

[17] Gómez, G., Koon, W.S., Lo, M.W., Marsden, J.E., Masdemont, J., Ross, S.D. Connecting orbits and invariant manifolds in the spatial restricted three-body problem. *Nonlinearity*. **17**, 5, 1571-1606 (2004).

[18] Gómez, G., Masdemont, J.J., Mondelo, J.M. Solar system models with a selected set of frequencies. *Astronomy & Astrophysics*. **390**, 2, 733-749 (2002).

[19] Gómez, G., Masdemont, J.J., Simó, C., Quasi-halo orbits associated with libration points. *J. Astron. Sci.*. **46**, 2, 1-42 (1999).

[20] Guzzo, M. Fourier analysis of chaotic motions and applications to Celestial Mechanics. In: Steves, B.A., Maciejewski, A.J., Hendry, M. (eds) Chaotic Worlds: From Order to Disorder in Gravitational *N*-Body Dynamical Systems. Nato Science series II-Vol. 227 (2006).

[21] Horrocks, J. Opera Posthuma. London (1673).

[22] Howell, K.C. Three-dimensional, periodic, 'halo' orbits. *Celestial Mechanics*. **32**, 53-71 (1984).

[23] Koon, W.S., Lo, M.W., Marsden J.E., Ross, S.D. *Dynamical Systems, the Three-Body Problem and Space Mission Design*. Available at `https://ross.aoe.vt.edu/books/` (2022).

[24] Laskar, J. Frequency analysis for multi-dimensional systems. Global dynamics and diffusion. *Physica D*. **67**, 1-3, 257-281 (1993).

[25] Laskar, J. Large scale chaos and marginal stability in the solar system. *Celest Mech Dyn Ast* **64**, 115-162 (1996).

[26] Lee, D.E. White Paper: Gateway Destination Orbit Model: A Continous 15 Year NRHO Reference Trajectory. Technical Report Document ID: 20190030294, NASA Johnson Space Center, Houston, TX (2019).

[27] Lian, Y., Gómez, G., Masdemont, J.J., Tang, G. A note on the dynamics around the Lagrange collinear points of the Earth–Moon system in a complete Solar System model. *Celest Mech Dyn Astr*, **115**, 185-211 (2013).

[28] McCarthy, B., Howell, K.C. Construction of Heteroclinic Connections Between Quasi-Periodic Orbits in the Three-Body Problem. *The Journal of the Astronautical Sciences*. **70**, 24 (2023).

[29] NASA/JPL Solar System Dynamics, JPL Horizons online solar system data and ephemeris computation service. Jet Propulsion Laboratory (JPL), California Institute of Technology. `https://ssd.jpl.nasa.gov/horizons/` (2025).

[30] Neugebauer, O. *A History of Ancient Mathematical Astronomy*. Springer, Berlin (1992).

[31] Park, B., Howell, K.C. Assessment of dynamical models for transitioning from the Circular Restricted Three-Body Problem to an ephemeris model with applications. *Celestial Mechanics and Dynamical Astronomy*. **136**, 6 (2024).

[32] Park, B., Howell, K.C., Stewart, S. A frequency-domain differential corrector for quasi-periodic trajectory design and analysis. *Physica D*. **482**, 134882 (2025).

[33] Park, B., Sanaga, R.R., Howell, K.C. A frequency-based hierarchy of dynamical models in cislunar space: leveraging periodically and quasi-periodically perturbed models. *Celest. Mech. Dyn. Astron.* **137**, 5 (2025).

[34] Park R.S., Folkner W.M., Williams J.G., Boggs D.H. The JPL Planetary and Lunar Ephemerides DE440 and DE441, The Astronomical Journal, **161**, 3, ID 105 (2021).

[35] Peterson, L.T., Rosales, J.J., Scheeres, D.J. The vicinity of Earth-Moon L_1 and L_2 in the Hill restricted 4-body problem. *Physica D*. **455**, 133889 (2023).

[36] Pollard, H. *Celestial Mechanics*. The Mathematical Association of America (1976).

[37] Qiao, C., Long, X., Yang, L., Zhu, Y., Cai, W. Calculation of a Dynamical Substitute for the Real Earth–Moon System Based on Hamiltonian Analysis. *The Astrophysical Journal*. **991**, 46 (2025).

[38] Richardson, D., Analytical construction of periodic orbits about the collinear points. *Celestial Mech.*, **22**, 3, 241-253 (1980).

[39] Rosales, J.J., Jorba, À., Jorba-Cuscó, M. Invariant manifolds near L_1 and L_2 in the quasi-bicircular problem. *Celestial Mechanics and Dynamical Astronomy*. **135**, 15 (2023).

[40] Roy, A.E. The use of the Saros in lunar dynamical studies. *The Moon*. **7**, 6-13 (1973).

[41] Roy, A.E. Orbital Motion, Taylor Francis Group (2005).

[42] Roy, A.E., Ovenden, M.W. On the Occurrence of Commensurable Mean Motions in the Solar System: The Mirror Theorem. *Monthly Notices of the Royal Astronomical Society*. **115**, 3, 296-309 (1955).

[43] Sanaga, R.R., Howell, K.C. Leveraging the Hill restricted four-body problem to investigate the ephemeris transition characteristics in the Earth-Moon L_2 halo orbit region. *Astrodynamics*. **9**, 785-805 (2025).

[44] Saros Series Catalog of Solar Eclipses, "Eclipse Predictions by Fred Espenak (NASA's GSFC)", `https://eclipse.gsfc.nasa.gov/SEsaros/SEsaros136.html`.

[45] Scantamburlo, E., Guzzo, M. Short-period effects of the planetary perturbations on the Sun-Earth Lagrangian point L_3. *Astronomy & Astrophysics*. **638**, A137 (2020).

[46] Scheeres, D.J. The Restricted Hill Four-Body Problem with Applications to the Earth-Moon-Sun system. *Celestial Mechanics and Dynamical Astronomy*. **70**, 75-98 (1998).

[47] Steves, B.A. The cycles of Selene. *Vistas in Astronomy*. **41**, 4, 543-571 (1997).

[48] The Astronomical Almanac for the Year 2019. U.S. Naval Observatory and Her Majesty's Nautical Almanac Office (2018).

[49] Valsecchi, G. B., Perozzi, E., Roy, A. E., Steves, B. A. Periodic orbits close to that of the Moon,*Astronomy & Astrophysics*, **271**, 308-314 (1993).

Extended Data Table 1. The 16 Mirror Configurations (MCs) possible in the Circular Restricted 3-Body Problem (CR3BP), and in the Circular Main Lunar Problem (CMLP).

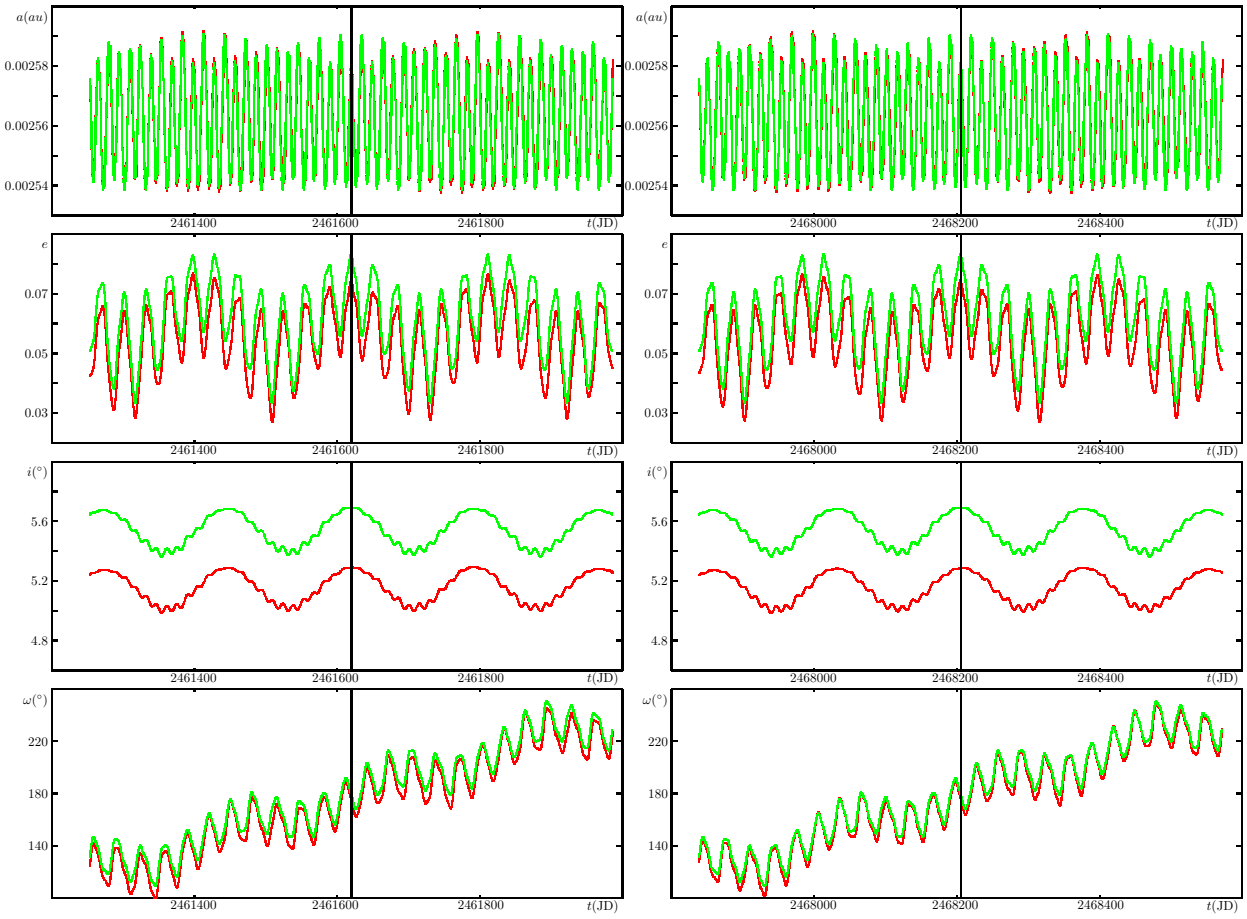
Colinear MCs	ω	f	$\Delta\lambda$	Coplanar MCs	ω	f	$\Delta\lambda$
000	0°	0°	0°	100	90°	0°	0°
002	0°	0°	180°	102	90°	0°	180°
020	0°	180°	0°	120	90°	180°	0°
022	0°	180°	180°	122	90°	180°	180°
200	180°	0°	0°	300	270°	0°	0°
202	180°	0°	180°	302	270°	0°	180°
220	180°	180°	0°	320	270°	180°	0°
222	180°	180°	180°	322	270°	180°	180°

Extended Data Table 2. Orbital elements of the Moon in the Mirror Configurations 200 and 022 in the Circular Restricted 3-Body Problem (CR3BP), and in the Circular Main Lunar Problem (CMLP). More details and a full derivation will be given in a forthcoming publication.

Model	MC	a	e	$i(^\circ)$
CR3BP	200	0.002 580 997 16	0.083 356 670	5.690 814 6
CMLP	200	0.002 580 994 90	0.083 364 192	5.690 661 3
CR3BP	022	0.002 590 632 07	0.056 488 496	5.688 171 3
CMLP	022	0.002 590 634 83	0.056 495 519	5.688 016 2

Extended Data Table 3. Frequencies and periods of the five sidereal longitudes describing the lunar and solar geocentric motions and of the four basic frequencies of the lunar geocentric motion with the corresponding periods and multiplicity (N) in the Saros. The first five lines give the frequencies, in radians per day and in degrees per day, as well as the periods in days, of the geocentric longitudes of Moon and Sun, of the geocentric longitudes of perigee and node of the Moon, and of the perigee of the Sun; the last four lines give the same values for $\Delta\lambda$, σ, ω and $\Delta\varpi$ and, in the last column, the number of times that the period is contained in a Saros. All the values presented in this Table are computed from the values of the anomalistic, sidereal and nodical months and the value of the sidereal year taken from[48], except the period of ϖ' which is taken from Table 1 of[25].

	Frequency (rad/d)	Frequency (°/d)	Period (d)	Number in Saros
$\dot\lambda$	0.229 970 83	13.176 358	27.321 662	
$\dot\lambda'$	0.017 202 124 16	0.985 609 113	365.256 363	
$\dot\varpi$	0.001 943 690 7	0.111 365 27	3 232.605 5	
$\dot\Omega$	−0.000 924 884 55	−0.052 991 981	−6 793.480 7	
$\dot\varpi'$	0.000 000 230 49	0.000 013 206	27 260 100.	
$\Delta\dot\lambda = \dot\lambda - \dot\lambda'$	0.212 768 71	12.190 749	29.530 589	223.000
$\dot\sigma = \dot\lambda' - \dot\varpi$	0.015 258 433	0.874 243 84	411.784 43	15.992
$\dot\omega = \dot\varpi - \dot\Omega$	0.002 868 575 3	0.164 357 26	2 190.350 5	3.007
$\Delta\dot\varpi = \dot\varpi - \dot\varpi'$	0.001 943 460 2	0.111 352 07	3 232.988 9	2.037



Extended Data Fig.1. Time evolutions of the orbital elements of the real Moon (red), taken from JPL DE 440[34], and the Moon in the periodic orbit 200-022 computed using the CMLP (green). From top to bottom the orbital elements are the semi-major axis (a), eccentricity (e), inclination (i), and argument of perigee (ω). Left column: The data for the real Moon are centered on 2.421487 August 2027, start on 1.242183 August 2026, and end on 3.585144 August 2028. The black vertical lines are set at 2.421487 August 2027, the date of the total solar eclipse in which the Moon will be close to the MC 200. Right column: the data for the real Moon are centered on 12.742834 August 2045, exactly 1 Saros of 6585.321347 d later than for the left column; they start on 11.563530 August 2044, and end on 14.906491 August 2046. The black vertical lines are set at 12.742834 August 2045, the date of the total solar eclipse in which the Moon will again be close to the MC 200.

Extended Data Table 4. Periods, peak-amplitudes (in au multiplied by 10^3) and the multiplicity N in the Saros, detected in the coordinate y of the real Moon and of the Saros-periodic orbit 200-022 computed in the CMLP represented in the S-EM reference frame (see Section Methods for details).

Real Moon			Periodic orbit 200-022		
Period	Half-ampl.	N	Period	Half-ampl.	N
29.530 590	1.290 434	223.000	29.530 589	1.289 808	223.000
411.784 346	0.084 540	15.992	411.582 583	0.095 365	16.000
14.254 184	0.035 326	461.992	14.253 942	0.039 813	462.000
32.128 088	0.034 841	204.971			
27.321 681	0.012 507	241.029			
15.314 422	0.007 769	430.008	15.314 701	0.008 759	430.000
25.231 376	0.002 783	260.997	25.231 117	0.003 202	261.000
9.843 530	0.002 531	669.000	9.843 530	0.002 696	669.000
193.564 615	0.001 590	34.021			
25.826 378	0.001 503	254.984	25.824 790	0.001 909	255.000
9.394 392	0.001 446	700.984	9.394 182	0.001 838	701.000
14.833 036	0.001 182	443.963			
35.226 615	0.000 868	186.942			
3 232.768 545	0.000 791	2.037			
15.984 617	0.000 572	411.979			
13.718 810	0.000 515	480.021			
7.252 619	0.000 248	907.992	7.252 557	0.000 293	908.000
10.116 154	0.000 244	650.971			
34.475 301	0.000 220	191.016	34.478 123	0.000 278	191.000
14.765 301	0.000 195	446.001	14.765 294	0.000 196	446.000
14.071 043	0.000 147	468.005	14.071 199	0.000 190	468.000
299.261 474	0.000 137	22.005	299.332 789	0.000 178	22.000
14.698 164	0.000 123	448.037			
35.595 746	0.000 108	185.003	35.596 332	0.000 125	185.000
13.170 920	0.000 090	499.989	13.170 643	0.000 117	500.000
23.601 062	0.000 073	279.026			
27.555 798	0.000 072	238.981	27.553 646	0.000 082	239.000
7.005 836	0.000 070	939.976	7.005 661	0.000 100	940.000
10.337 770	0.000 065	637.016	10.338 024	0.000 083	637.000
365.269 064	0.000 065	18.029			
13.331 245	0.000 060	493.976	13.330 610	0.000 086	494.000
9.642 389	0.000 057	682.955			
7.517 423	0.000 052	876.008	7.517 490	0.000 061	876.000
31.806 462	0.000 051	207.044	31.813 466	0.000 058	207.000
9.585 209	0.000 051	687.029			

Extended Data Table 5. Identification of the frequencies in the lunar orbit, coordinate x.

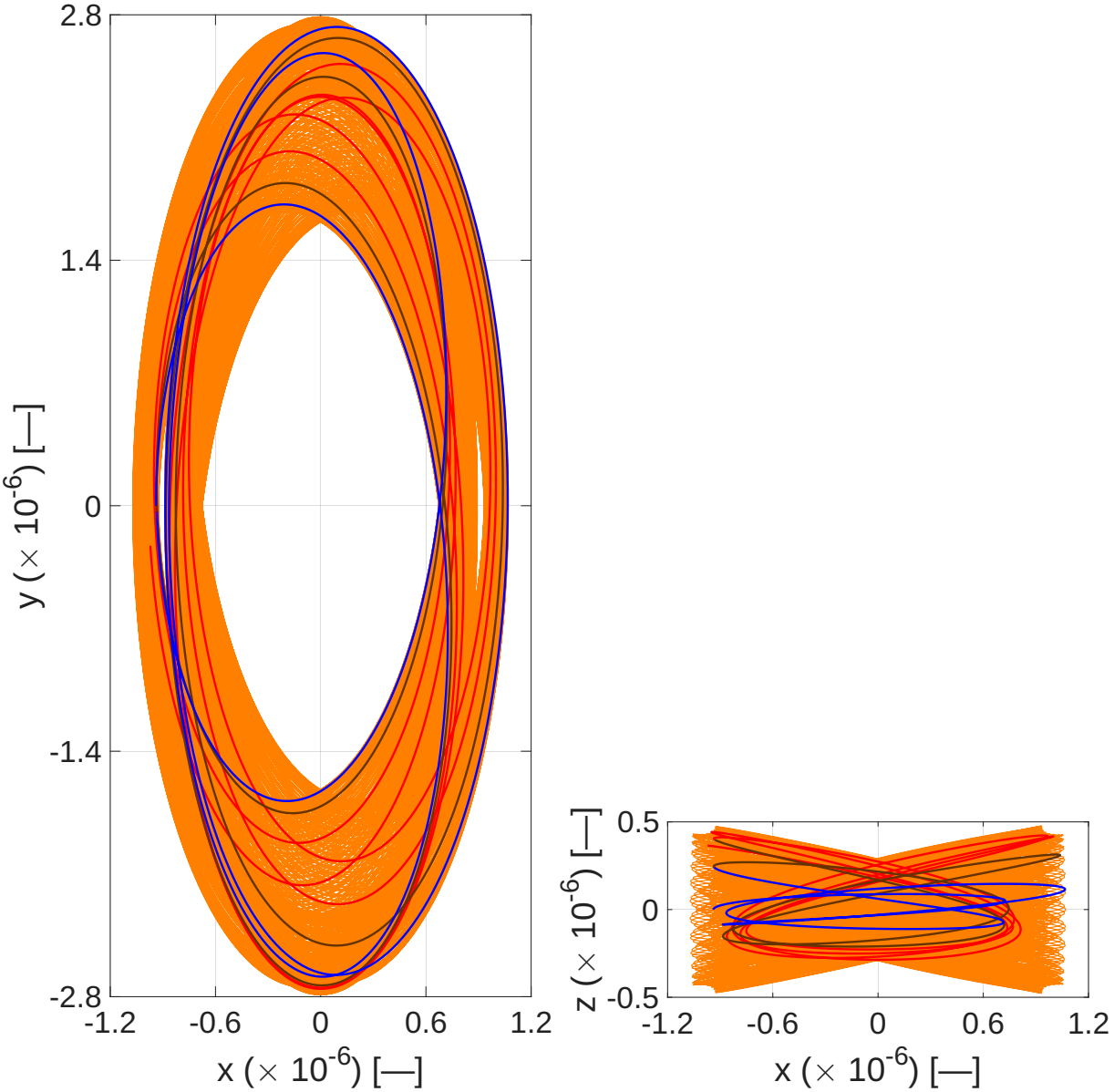
Period	Revs	In PO?	Key	Frequency
29.530 590	223.000	Yes	223	$\dot{\lambda}-\dot{\lambda}'$
411.784 357	15.992	Yes	16	$\dot{\lambda}'-\dot{\varpi}$
14.254 184	461.992	Yes	$2\cdot223+16$	$2\dot{\lambda}-\dot{\lambda}'-\dot{\varpi}$
32.128 088	204.971	No	$223-16-2.037$	$\dot{\lambda}-2\dot{\lambda}'+\dot{\varpi}'$
27.321 680	241.029	No	$223+16+2.037$	$\dot{\lambda}-\dot{\varpi}'$
15.314 422	430.008	Yes	$2\cdot223-16$	$2\dot{\lambda}-3\dot{\lambda}'+\dot{\varpi}$
193.564 621	34.021	No	$2\cdot16+2.037$	$2\dot{\lambda}'-\dot{\varpi}-\dot{\varpi}'$
9.843 530	669.000	Yes	$3\cdot223$	$3\dot{\lambda}-3\dot{\lambda}'$
25.231 371	260.997	Yes	$223+2\cdot16+2\cdot3$	$\dot{\lambda}+\dot{\lambda}'-2\dot{\Omega}$
9.394 392	700.984	Yes	$3\cdot223+2\cdot16$	$3\dot{\lambda}-\dot{\lambda}'-2\dot{\varpi}$
14.833 036	443.963	No	$2\cdot223-2.037$	$2\dot{\lambda}-2\dot{\lambda}'-\dot{\varpi}+\dot{\varpi}'$
35.226 616	186.942	No	$223-2\cdot16-2.037$	$\dot{\lambda}-3\dot{\lambda}'+\dot{\varpi}'$
15.984 617	411.979	No	$2\cdot223-2\cdot16-2.037$	$2\dot{\lambda}-4\dot{\lambda}'+\dot{\varpi}+\dot{\varpi}'$
13.718 810	480.021	No	$2\cdot223+2\cdot16+2.037$	$2\dot{\lambda}-\dot{\varpi}-\dot{\varpi}'$
25.826 377	254.984	Yes	$223+2\cdot16$	$\dot{\lambda}+\dot{\lambda}'-2\dot{\varpi}$
34.475 299	191.016	Yes	$223-2\cdot16$	$\dot{\lambda}-3\dot{\lambda}'+2\dot{\varpi}$
7.252 619	907.992	Yes	$4\cdot223+16$	$4\dot{\lambda}-3\dot{\lambda}'-\dot{\varpi}$
10.116 154	650.971	No	$3\cdot223-16-2.037$	$3\dot{\lambda}-4\dot{\lambda}'+\dot{\varpi}'$
299.261 431	22.005	Yes	$16+2\cdot3$	$\dot{\lambda}'+\dot{\varpi}-2\dot{\Omega}$
14.765 299	446.000	Yes	$2\cdot223$	$2\dot{\lambda}-2\dot{\lambda}'$
14.698 164	448.037	No	$2\cdot223+2.037$	$2\dot{\lambda}-2\dot{\lambda}'+\dot{\varpi}-\dot{\varpi}'$
14.071 043	468.005	Yes	$2\cdot223+16+2\cdot3$	$2\dot{\lambda}-\dot{\lambda}'+\dot{\varpi}-2\dot{\Omega}$
35.595 753	185.003	Yes	$223-2\cdot16-2\cdot3$	$\dot{\lambda}-3\dot{\lambda}'+2\dot{\Omega}$
126.518 668	52.050	No	$3\cdot16+2\cdot2.037$	$3\dot{\lambda}'-\dot{\varpi}-2\dot{\varpi}'$
365.276 159	18.028	No	$16+2.037$	$\dot{\lambda}'-\dot{\varpi}'$
7.005 836	939.976	Yes	$4\cdot223+3\cdot16$	$4\dot{\lambda}-\dot{\lambda}'-3\dot{\varpi}$
10.337 770	637.016	Yes	$3\cdot223-2\cdot16$	$3\dot{\lambda}-5\dot{\lambda}'+2\dot{\varpi}$
27.555 979	238.980	Yes	$223+16$	$\dot{\lambda}-\dot{\varpi}$
3 232.910 076	2.037	No	2.037	$\dot{\varpi}-\dot{\varpi}'$
23.601 095	279.026	No	$223+3\cdot16+2\cdot3+2.037$	$\dot{\lambda}+2\dot{\lambda}'-\dot{\varpi}'-2\dot{\Omega}$
9.642 389	682.955	No	$3\cdot223+16-2.037$	$3\dot{\lambda}-2\dot{\lambda}'-2\dot{\varpi}+\dot{\varpi}'$
25.420 251	259.058	No	$223+2\cdot16+2\cdot2.037$	$\dot{\lambda}+\dot{\lambda}'-2\dot{\varpi}'$
7.517 423	876.008	Yes	$4\cdot223-16$	$4\dot{\lambda}-5\dot{\lambda}'+\dot{\varpi}$
13.170 918	499.990	Yes	$2\cdot223+3\cdot16+2\cdot3$	$2\dot{\lambda}+\dot{\lambda}'-\dot{\varpi}-2\dot{\Omega}$
9.585 210	687.029	No	$3\cdot223+16+2.037$	$3\dot{\lambda}-2\dot{\lambda}'-\dot{\varpi}'$

Extended Data Table 6. Identification of the frequencies in the lunar orbit, coordinate y.

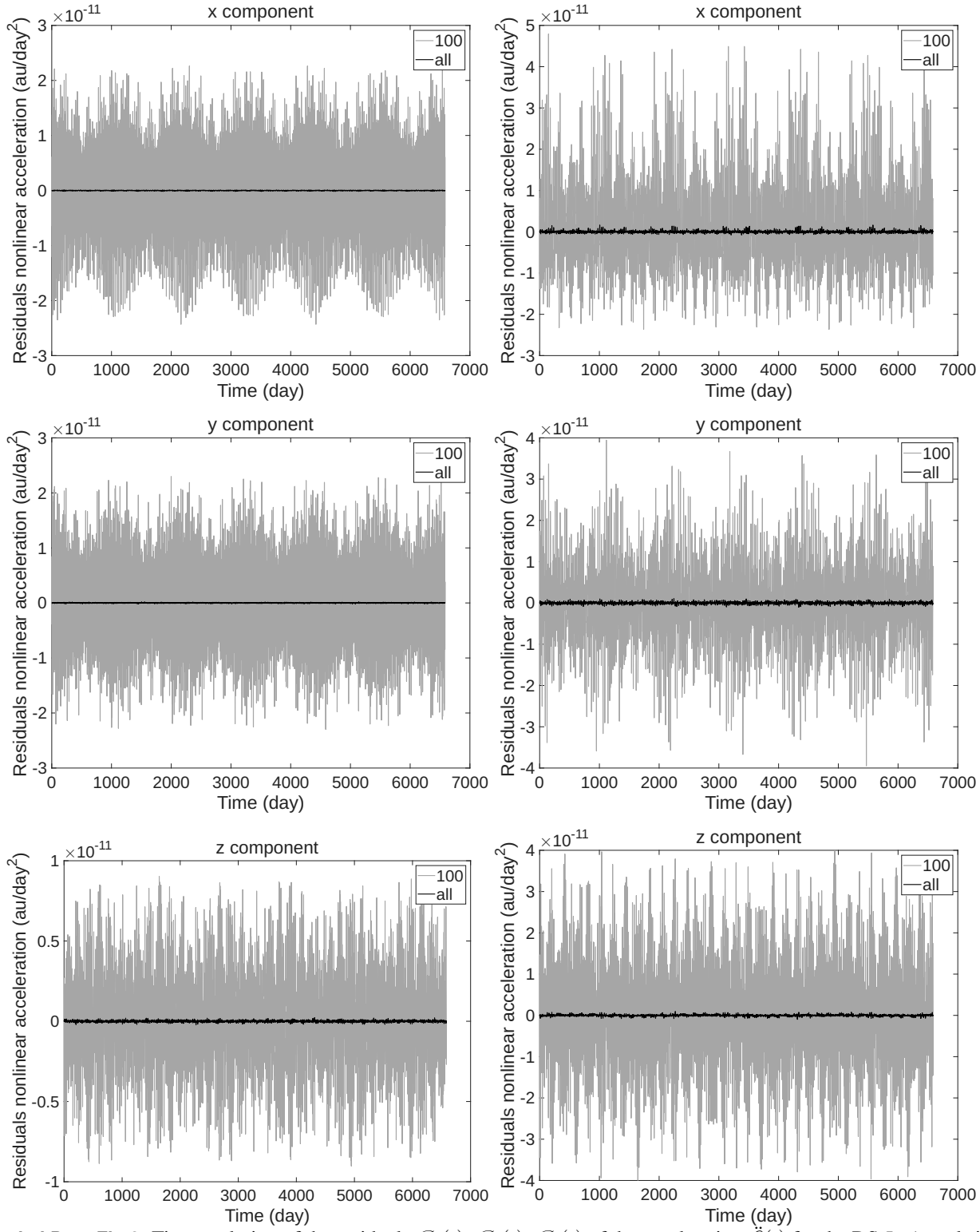
Period	Revs	In PO?	Key	Frequency
29.530 590	223.000	Yes	223	$\dot\lambda - \dot\lambda'$
411.784 346	15.992	Yes	16	$\dot\lambda' - \dot\varpi$
14.254 184	461.992	Yes	$2\cdot 223 + 16$	$2\dot\lambda - \dot\lambda' - \dot\varpi$
32.128 088	204.971	No	$223 - 16 - 2.037$	$\dot\lambda - 2\dot\lambda' + \dot\varpi'$
27.321 681	241.029	No	$223 + 16 + 2.037$	$\dot\lambda - \dot\varpi'$
15.314 422	430.008	Yes	$2\cdot 223 - 16$	$2\dot\lambda - 3\dot\lambda' + \dot\varpi$
25.231 376	260.997	Yes	$223 + 2\cdot 16 + 2\cdot 3$	$\dot\lambda + \dot\lambda' - 2\dot\Omega$
9.843 530	669.000	Yes	$3\cdot 223$	$3\dot\lambda - 3\dot\lambda'$
193.564 615	34.021	No	$2\cdot 16 + 2.037$	$2\dot\lambda' - \dot\varpi - \dot\varpi'$
25.826 378	254.984	Yes	$223 + 2\cdot 16$	$\dot\lambda + \dot\lambda' - 2\dot\varpi$
9.394 392	700.984	Yes	$3\cdot 223 + 2\cdot 16$	$3\dot\lambda - \dot\lambda' - 2\dot\varpi$
14.833 036	443.963	No	$2\cdot 223 - 2.037$	$2\dot\lambda - 2\dot\lambda' - \dot\varpi + \dot\varpi'$
35.226 615	186.942	No	$223 - 2\cdot 16 - 2.037$	$\dot\lambda - 3\dot\lambda' + \dot\varpi'$
3 232.768 545	2.037	No	2.037	$\dot\varpi - \dot\varpi'$
15.984 617	411.979	No	$2\cdot 223 - 2\cdot 16 - 2.037$	$2\dot\lambda - 4\dot\lambda' + \dot\varpi + \dot\varpi'$
13.718 810	480.021	No	$2\cdot 223 + 2\cdot 16 + 2.037$	$2\dot\lambda - \dot\varpi - \dot\varpi'$
7.252 619	907.992	Yes	$4\cdot 223 + 16$	$4\dot\lambda - 3\dot\lambda' - \dot\varpi$
10.116 154	650.971	No	$3\cdot 223 - 16 - 2.037$	$3\dot\lambda - 4\dot\lambda' + \dot\varpi'$
34.475 301	191.016	Yes	$223 - 2\cdot 16$	$\dot\lambda - 3\dot\lambda' + 2\dot\varpi$
14.765 301	446.001	Yes	$2\cdot 223$	$2\dot\lambda - 2\dot\lambda'$
14.071 043	468.005	Yes	$2\cdot 223 + 16 + 2\cdot 3$	$2\dot\lambda - \dot\lambda' + \dot\varpi - 2\dot\Omega$
299.261 474	22.005	Yes	$16 + 2\cdot 3$	$\dot\lambda' + \dot\varpi - 2\dot\Omega$
14.698 164	448.037	No	$2\cdot 223 + 2.037$	$2\dot\lambda - 2\dot\lambda' + \dot\varpi - \dot\varpi'$
35.595 746	185.003	Yes	$223 - 2\cdot 16 - 2\cdot 3$	$\dot\lambda - 3\dot\lambda' + 2\dot\Omega$
13.170 920	499.989	Yes	$2\cdot 223 + 3\cdot 16 + 2\cdot 3$	$2\dot\lambda + \dot\lambda' - \dot\varpi - 2\dot\Omega$
23.601 062	279.026	No	$223 + 3\cdot 16 + 2\cdot 3 + 2.037$	$\dot\lambda + 2\dot\lambda' - \dot\varpi' - 2\dot\Omega$
27.555 798	238.981	Yes	$223 + 16$	$\dot\lambda - \dot\varpi$
7.005 836	939.976	Yes	$4\cdot 223 + 3\cdot 16$	$4\dot\lambda - \dot\lambda' - 3\dot\varpi$
10.337 770	637.016	Yes	$3\cdot 223 - 2\cdot 16$	$3\dot\lambda - 5\dot\lambda' + 2\dot\varpi$
365.269 064	18.029	No	$16 + 2.037$	$\dot\lambda' - \dot\varpi'$
13.331 245	493.976	Yes	$2\cdot 223 + 3\cdot 16$	$2\dot\lambda + \dot\lambda' - 3\dot\varpi$
9.642 389	682.955	No	$3\cdot 223 + 16 - 2.037$	$3\dot\lambda - 2\dot\lambda' - 2\dot\varpi + \dot\varpi'$
7.517 423	876.008	Yes	$4\cdot 223 - 16$	$4\dot\lambda - 5\dot\lambda' + \dot\varpi$
31.806 462	207.044	Yes	$223 - 16$	$\dot\lambda - 2\dot\lambda' + \dot\varpi$
9.585 209	687.029	No	$3\cdot 223 + 16 + 2.037$	$3\dot\lambda - 2\dot\lambda' - \dot\varpi'$

Extended Data Table 7. Identification of the frequencies in the lunar orbit, coordinate z.

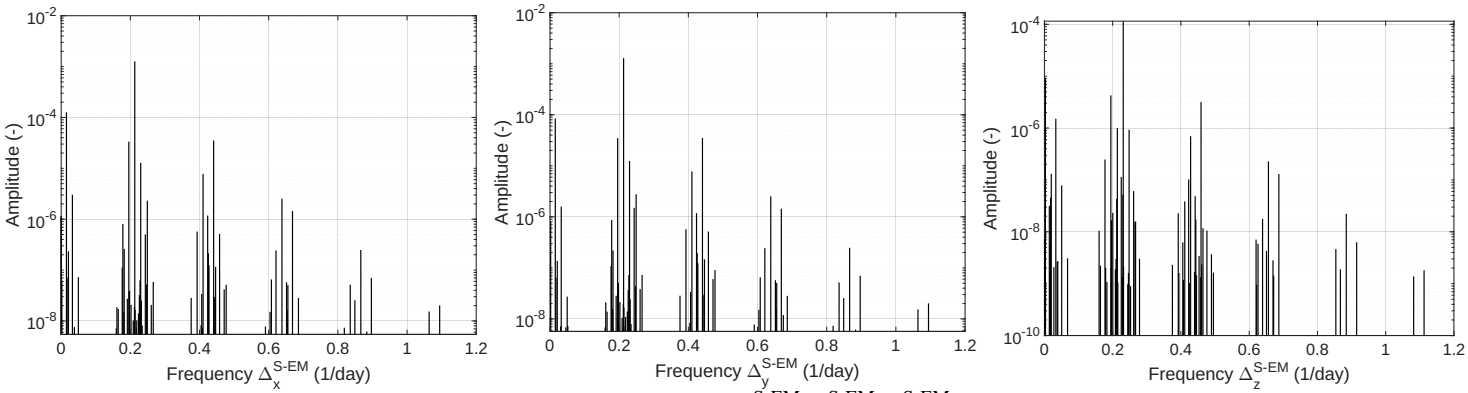
Period	Revs	In PO?	Key	Frequency
27.212 221	241.999	Yes	$223+16+3$	$\dot{\lambda}-\dot{\Omega}$
2 190.319 549	3.007	Yes	3	$\dot{\varpi}-\dot{\Omega}$
32.280 778	204.001	Yes	$223-16-3$	$\dot{\lambda}-2\dot{\lambda}'+\dot{\Omega}$
13.691 158	480.991	Yes	$2\cdot 223+2\cdot 16+3$	$2\dot{\lambda}-\dot{\varpi}-\dot{\Omega}$
188.201 314	34.991	Yes	$2\cdot 16+3$	$2\dot{\lambda}'-\dot{\varpi}-\dot{\Omega}$
29.402 755	223.970	No	$223+3-2.037$	$\dot{\lambda}-\dot{\lambda}'-\dot{\Omega}+\dot{\varpi}'$
25.325 450	260.028	No	$223+2\cdot 16+3+2.037$	$\dot{\lambda}+\dot{\lambda}'-\dot{\Omega}-\dot{\varpi}'$
14.666 428	449.006	Yes	$2\cdot 223+3$	$2\dot{\lambda}-2\dot{\lambda}'+\dot{\varpi}-\dot{\Omega}$
35.410 248	185.972	No	$223-2\cdot 16-3-2.037$	$\dot{\lambda}-3\dot{\lambda}'+\dot{\Omega}+\dot{\varpi}'$
9.571 707	687.999	Yes	$3\cdot 223+16+3$	$3\dot{\lambda}-2\dot{\lambda}'-\dot{\Omega}$
313.059 023	21.035	No	$16+3+2.037$	$\dot{\lambda}'+\dot{\varpi}-\dot{\Omega}-\dot{\varpi}'$
9.146 496	719.983	Yes	$3\cdot 223+3\cdot 16+3$	$3\dot{\lambda}-2\dot{\varpi}-\dot{\Omega}$
27.905 587	235.986	Yes	$223+16-3$	$\dot{\lambda}-2\dot{\varpi}+\dot{\Omega}$
14.865 504	442.993	Yes	$2\cdot 223-3$	$2\dot{\lambda}-2\dot{\lambda}'-\dot{\varpi}+\dot{\Omega}$
124.204 480	53.020	No	$3\cdot 16+3+2.037$	$3\dot{\lambda}'-\dot{\varpi}-\dot{\Omega}-\dot{\varpi}'$
24.035 515	273.983	Yes	$223+3\cdot 16+3$	$\dot{\lambda}+2\dot{\lambda}'-2\dot{\varpi}-\dot{\Omega}$
27.321 609	241.030	No	$223+16+2.037$	$\dot{\lambda}-\dot{\varpi}'$



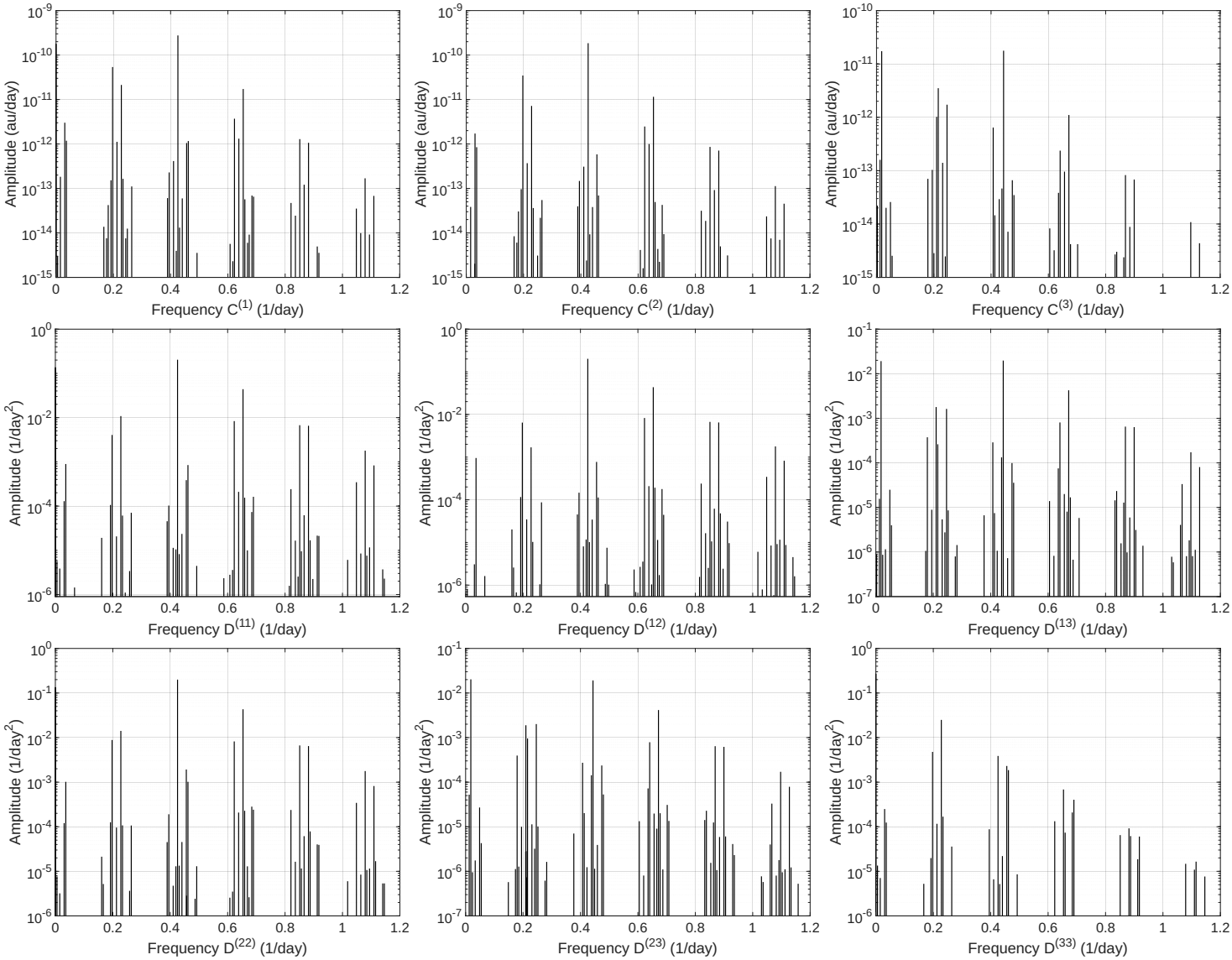
Extended Data Fig.2. Projections of the DS L_1 on the x-y (top-left) and x-z (top-right) planes of a reference frame centered at the formal Lagrangian solution and rotating-pulsating to maintain the Earth and the Moon on the x axis, with mutual distance equal to 1. The projected curves are represented in orange along a full Saros cycle, in blue, brown along the first and second synodic months, and in red along the third and fourth synodic months. The DS is computed using $N_S = 406$ frequencies.



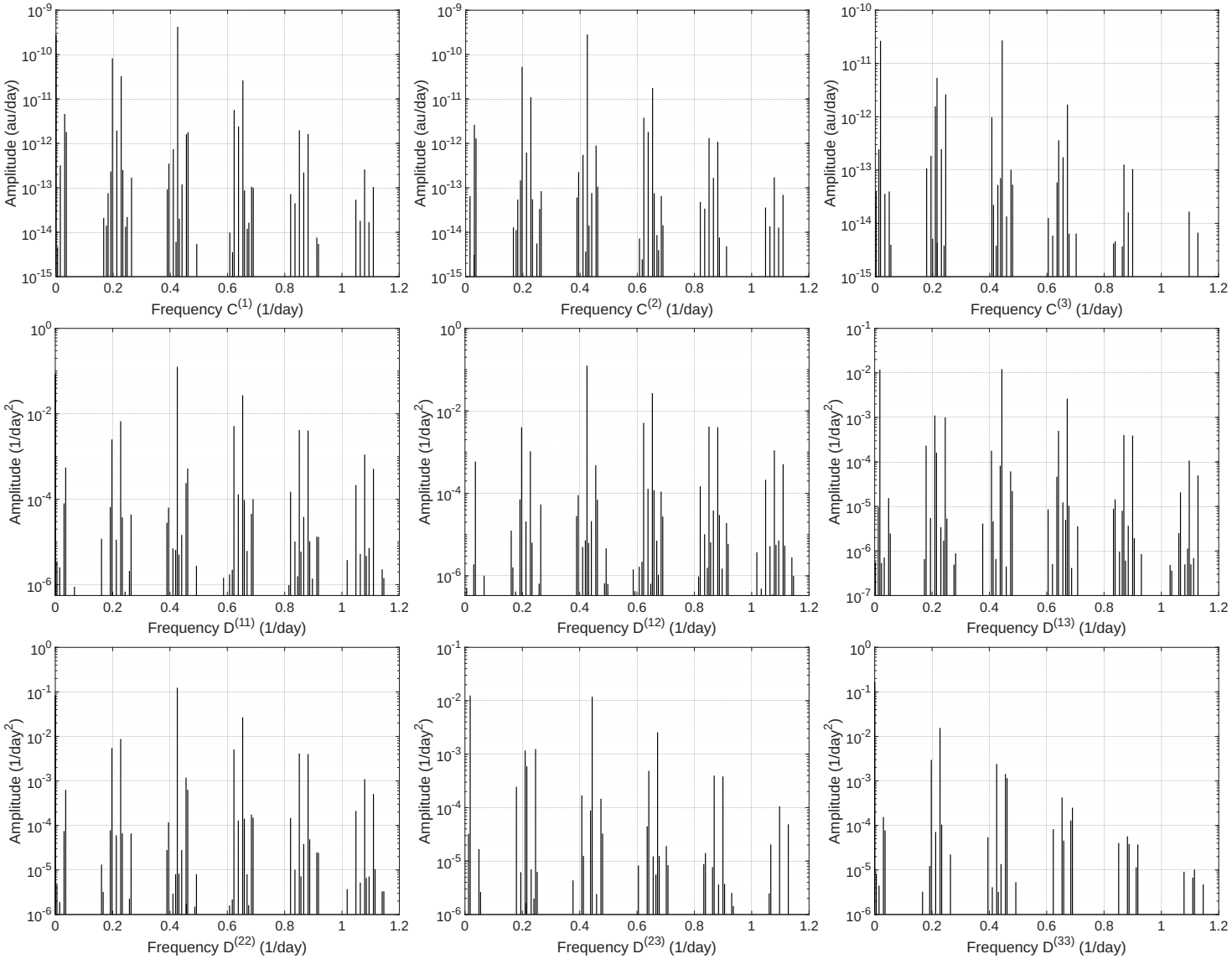
Extended Data Fig.3. Time evolution of the residuals $\mathscr{R}_x(t)$, $\mathscr{R}_y(t)$, $\mathscr{R}_z(t)$ of the acceleration $\ddot{\mathscr{E}}(t)$ for the DS L_1 (panels in the right-column) and for DS L_2 (panels in the left-column) with respect to the nonlinear acceleration F (see Eq. 8). Two different numbers of frequencies for $\mathscr{E}(t)$ are considered: $N_S = 190$ and the maximum number of frequencies $N_S = 406$ for L_1; $N_S = 100$ and the maximum number of frequencies $N_S = 558$ for L_2.



Extended Data Fig.4. Spectrum of the Cartesian components $\Delta_x^{\text{S-EM}}, \Delta_y^{\text{S-EM}}, \Delta_z^{\text{S-EM}}$ of the real orbit of the Moon in the S-EM reference frame. The frequencies are expressed in rad/d, while the amplitudes are normalized by distance of the Sun from the barycenter of the Earth and Moon.



Extended Data Fig.5. Fourier spectra of the components of the vector $C(t)$ and entries of the symmetric matrix $D(t)$, computed from Eqs. (14) and (15), respectively, for L_1. The norm of the amplitudes and the (positive) frequencies are obtained from the NAFF.



Extended Data Fig.6. Fourier spectra of the components of the vector $C(t)$ and entries of the symmetric matrix $D(t)$, computed from Eqs. (14) and (15), respectively, for L_2. The norm of the amplitudes and the (positive) frequencies are obtained from the NAFF.